Journal of Sound and Vibration (2001) **245**(5), 877–913
doi:10.1006/jsvi.2001.3617, available online at http://www.idealibrary.com on IDEAL®

MULTI-DIMENSIONAL CHARACTERIZATION OF VIBRATION ISOLATORS OVER A WIDE RANGE OF FREQUENCIES

S. KIM AND R. SINGH

Acoustics and Dynamics Laboratory, Department of Mechanical Engineering and The Center for Automotive Research, The Ohio State University, Columbus, OH 43210-1107, *U.S.A.*
E-mail: singh.3@osu.edu

(*Received* 26 *September* 2000, *and in final form* 11 *January* 2001)

This article presents a new experimental identification method for extracting frequency-dependent multi-dimensional dynamic stiffnesses of an isolator. The scope is limited to linear time-invariant system and analysis is performed only in the frequency domain. The proposed characterization method uses two inertial elements and an isolator, and a refined multi-dimensional mobility synthesis formulation is developed for estimating the properties of this system. For example, dynamic stiffnesses of an isolator are decomposed given the measured mobilities of the overall system and rigid body system theory. Approximate identification schemes for transfer dynamic stiffnesses, as proposed by prior researchers, are analytically examined for axial motions. The aforementioned approximate scheme is then extended to the identification of flexural stiffnesses. Both symmetric and asymmetric isolators are analyzed, based on a simulation example that models the isolator using a Euler beam and wave equation formulations for flexural and longitudinal motions respectively. Finally, the proposed identification method is applied to three rubber isolators up to 2 kHz, and transfer stiffness estimations are successfully compared with data measured on a commercial test machine for axial motions up to 1 kHz. Our method is very promising though its utility could be limited because of the zero preload assumption.
© 2001 Academic Press

1. INTRODUCTION

Experimental methods must be adopted to dynamically characterize stiffnesses of rubber, hydraulic, air and metallic isolators since they invariably exhibit frequency-dependent properties and are sensitive to mean loads and dynamic excitation levels [1, 2]. This is especially true for a visco-elastic material since the material properties are complex-valued and show frequency, temperature and strain dependence [2, 3]. Historically, characterization methods have focused on axial or compressional stiffness, since many vibration isolation measures consider only this component [1, 2, 4, 5]. Also, in most studies only the lower frequency range has been considered [6–8], and the direct measurement of dynamic stiffness on commercial machines is typically limited to lower frequencies due to resonances in the machine [9]. In this article, we propose a new dynamic characterization method that should be valid over a wide frequency range. Further, we introduce a new isolator stiffness matrix formulation. Various subsets of this concept will be examined and compared with existing experimental techniques [10, 11], as well with some recent literature [12, 13]. Given the complexity of issues, only the linear time-invariant formulation will be considered in this article. Consequently, the effects of preload, temperature and the like will be beyond the scope of the present work.

0022-460X/01/350877 + 37 $35.00/0 © 2001 Academic Press

2. EXPERIMENTAL CHARACTERIZATION ISSUES

Static stiffness can easily be measured using commercial (such as Instron and MTS) machines [9]. It is well known that dynamic properties differ from static properties, especially for elastomeric materials [1, 3]. A majority of prior studies have focused on the effect of compressional or axial stiffness of isolators [1, 2, 4, 5] since it has been regarded as a main contributor to the vibration transmission. For instance, Nielsen *et al.* [7] have proposed a method for the estimation of elastomeric material properties, based on the measurement of the driving point axial stiffness. Also, Jeong [8] has developed an identification method for axial and shear stiffnesses of an isolator based on a three-degree-of-freedom modal experiment. However, Sanderson [14] has shown that the rotational stiffness could be a significant contributor to the vibration transmission. Nonetheless, frequency-invariant stiffnesses were chosen in his study and the coupling stiffnesses in flexural motions were ignored. Rotational mobilities or stiffnesses of a structure can be identified by adding and subtracting translational responses, given harmonic excitation to a rigid body [15]. But, its identification is not straightforward for many real-life problems since the rotational components must be handled by a coupled formulation with lateral components in flexure [16].

Commercial equipment is available for the identification of cross-point dynamic stiffnesses in single and multi-axis motions, under various preloads. However, the use of such machines is mostly limited to lower frequencies [9]. In order to correctly predict the vibrational response of any structure, both driving point and transfer stiffnesses must be incorporated, especially when standing wave effects occur within the isolators. Such effects, when resulting from isolator inertial properties, tend to be pronounced when the frequency increases [2]. Therefore, approaches that neglect key differences between driving point and transfer stiffnesses may yield erroneous predictions, especially in the high-frequency regime.

Several approximate identification methods for transfer stiffness of resilient elements have been proposed for axial (compressional) motions at higher frequencies [10, 11]; these have been further refined for lower frequencies [12, 13]. One such approximate method has also been applied to the identification of flexural stiffnesses [12]. Recently, a new characterization method has also been proposed to examine the non-linear behavior of isolators at lower frequencies but it is also limited to axial motion [17]. Overall, an appropriate characterization method for the measurement of multi-dimensional stiffnesses of an isolator has yet to be proposed. The underlying measurement and estimation issues are even more difficult as the frequency increases [6, 7].

3. PROBLEM FORMULATION

Problem formulation is conceptually shown in Figure 1 where $\mathbf{V}_{Si}$, $\mathbf{V}_{Pi}$ and $\mathbf{V}_{Ri}$ are the velocity vectors for source (S), path (P) and receiver (R) respectively. Here $\mathbf{F}_{Si}$ is the force excitation vector at the source, $\mathbf{F}_{Pi}$ and $\mathbf{F}_{Ri}$ are the transmitted force vectors at the junction of source and path and at the junction of path and receiver respectively. Also, $\boldsymbol{\alpha}$, $\boldsymbol{\beta}$ and $\boldsymbol{\gamma}$ represent the mobility matrices ($\mathbf{M}$) of source, path and receiver respectively. The primary objectives of this study include the following: (1) propose an analytical framework, based on mobility synthesis method of Figure 1(b) that will synthesize or extract a multi-dimensional stiffness matrix at any given frequency (ω); (2) suggest a new experimental identification method for spectrally varying multi-dimensional properties of an isolator (in terms of mobility or stiffness); (3) apply the proposed identification scheme to one simulation

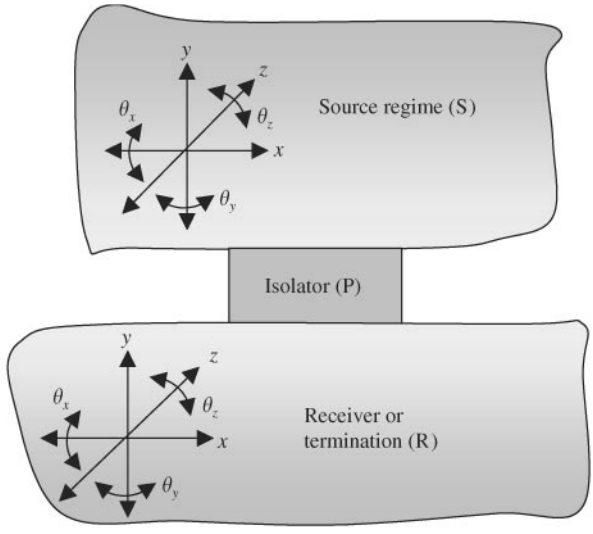

(a)

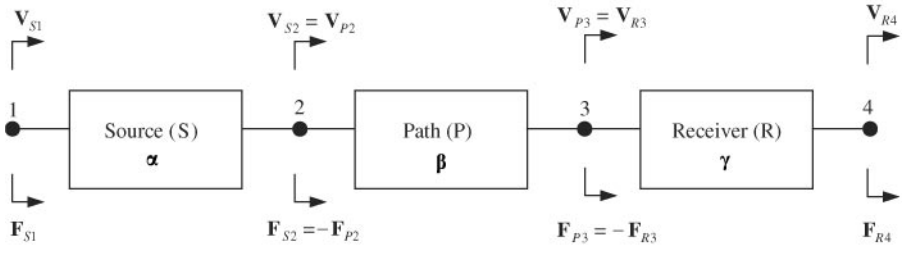

(b)

Figure 1. Problem formulation: (a) isolator is depicted as a multi-dimensional path for any practical problem; (b) source–path–receiver system and their mobility matrices $\boldsymbol{\alpha}$, $\boldsymbol{\beta}$, $\boldsymbol{\gamma}$. Here, $\mathbf{F}$ and $\mathbf{V}$ are vectors.

example and three isolator examples; (4) examine the methods proposed by Thompson *et al.* [10–13] and their underlying assumptions using analytical and numerical methods; and (5) validate the proposed identification scheme by comparing results with data measured on a commercial machine.

The scope is limited to a linear time-invariant (LTI) system, and the effects of preload, etc. are not considered. Frequency domain methods such as the mobility synthesis or transfer matrix techniques are well established for the analysis of a combined system given individual components [18–22]. The responses and interfacial forces for more than three-sub-systems systems can be obtained by numerically iterating the synthesis procedure based on two sub-systems. Nonetheless, an analytical expression for a combination of three (or more) sub-systems is still needed for some cases. For example, Sykes [22] has developed an analytical expression for multi-dimensional responses at the receiver input location of a source–path–receiver system but the excitation was expressed in terms of either a free velocity or a blocked force source. In our study, we examine a more general case. For the

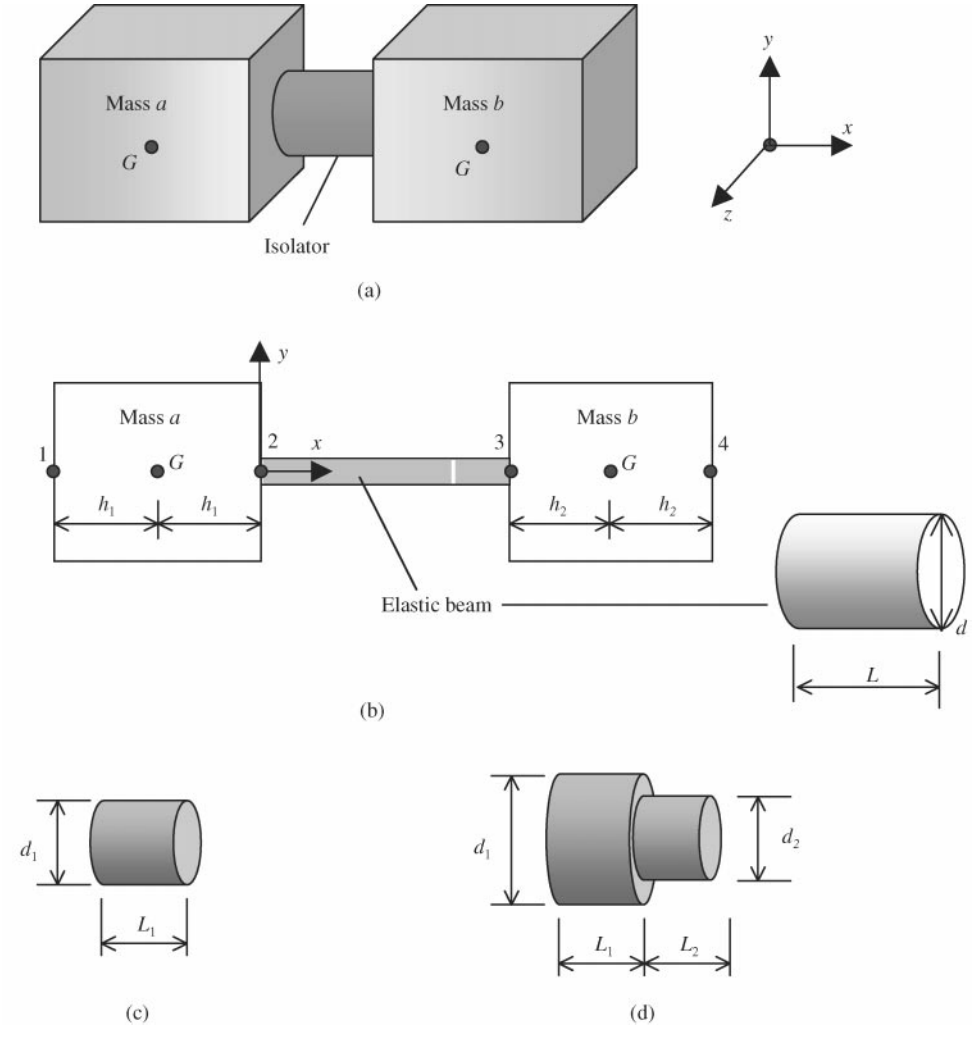

Figure 2. Proposed identification scheme. (a) schematic; (b) simulation example; (c) symmetric isolator used for simulation; (d) asymmetric isolator used for simulation.

identification of spectrally varying stiffness properties, refined multi-dimensional mobility synthesis and decomposition procedures will be formulated. Note that Sykes [22] did not consider the decomposition process. The proposed formulation is applied to extract the properties of an isolator from the measured response of a combined structure and then to decompose translational and rotational components of mobility. The experimental system of Figure 2(a), as proposed in our study, consists of two masses (simulating source and receiver) that are attached to either sides of an isolator. Refer to Figure 3 for lumped models of the system. The proposed method will be applied to three rubber isolators of Figure 4 and the mobility matrix for each isolator will be identified up to 2 kHz using the proposed method. A frequency range up to 2 kHz is chosen as an extension of the upper frequency limit of 1 kHz for our commercial machine (MTS 831.50).

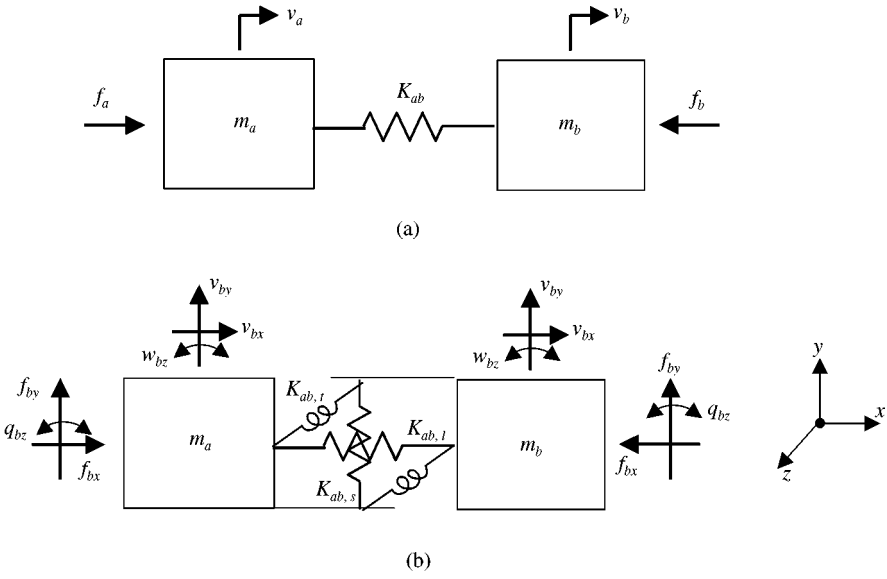

Figure 3. Lumped approximations of system of Figure 2(a). (a) isolator is modelled via a scalar stiffness in the axial direction; (b) isolator is described by multi-dimensional stiffness terms. Here, $K_{ab,l}$, $K_{ab,s}$ and $K_{ab,t}$ represent axial, shear and rotational stiffnesses respectively.

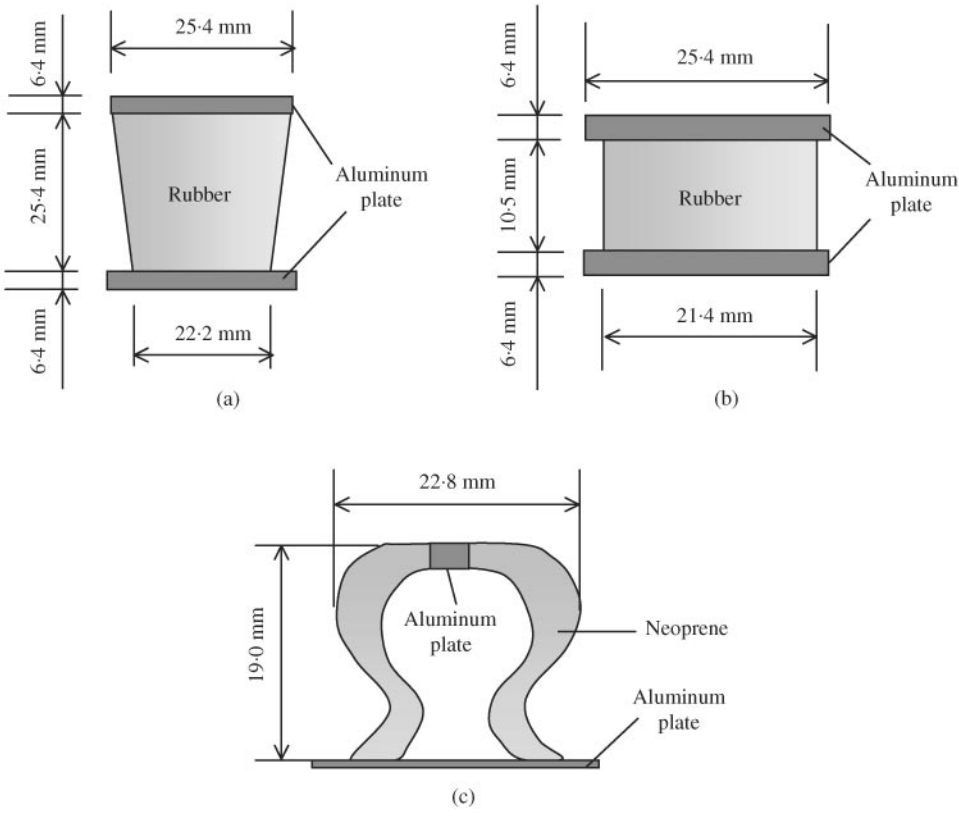

Figure 4. Rubber isolators used for experimental studies. (a) isolator 1; (b) isolator 2; (c) isolator 3.

4. MULTI-DIMENSIONAL MOBILITY SYNTHESIS FORMULATION

4.1. SOURCE, PATH AND RECEIVER SYSTEM

Harmonic velocity and interfacial force vectors between sub-systems can be expressed as follows, with reference to Figure 1(b):

$$\mathbf{V}_{S1} = \boldsymbol{\alpha}_{11}\mathbf{F}_{S1} + \boldsymbol{\alpha}_{12}\mathbf{F}_{S2}, \qquad \mathbf{V}_{S2} = \boldsymbol{\alpha}_{21}\mathbf{F}_{S1} + \boldsymbol{\alpha}_{22}\mathbf{F}_{S2}, \tag{1a, b}$$

$$\mathbf{V}_{P2} = \boldsymbol{\beta}_{22}\mathbf{F}_{P2} + \boldsymbol{\beta}_{23}\mathbf{F}_{P3}, \qquad \mathbf{V}_{P3} = \boldsymbol{\beta}_{32}\mathbf{F}_{P2} + \boldsymbol{\beta}_{33}\mathbf{F}_{P3}, \tag{1c, d}$$

$$\mathbf{V}_{R3} = \boldsymbol{\gamma}_{33}\mathbf{F}_{R3} + \boldsymbol{\gamma}_{34}\mathbf{F}_{R4}, \qquad \mathbf{V}_{R4} = \boldsymbol{\gamma}_{43}\mathbf{F}_{R3} + \boldsymbol{\gamma}_{44}\mathbf{F}_{R4}. \tag{1e, f}$$

Here, $\boldsymbol{\alpha}_{ij}$, $\boldsymbol{\beta}_{ij}$ and $\boldsymbol{\gamma}_{ij}$ represent the mobility matrices of source, path and receiver respectively and the ubiquitous (ω) term is dropped for the sake of brevity since only the frequency domain representation is considered. Also, refer to Appendix A for nomenclature. Synthesized formulation is obtained by using the motion compatibility $\mathbf{V}_i = \mathbf{V}_j$ and the force equilibrium $\mathbf{F}_i + \mathbf{F}_j = 0$ conditions at each interface (2 or 3). Force equilibrium and motion compatibility conditions for connecting locations are

$$\mathbf{V}_{S2} = \mathbf{V}_{P2}, \qquad \mathbf{V}_{P3} = \mathbf{V}_{R3}, \tag{2a, b}$$

$$\mathbf{F}_{S2} = -\mathbf{F}_{P2}, \qquad \mathbf{F}_{P3} = -\mathbf{F}_{R3}. \tag{2c, d}$$

Interfacial forces at location 2 are obtained by substituting equations (1b) and (1c) into equation (2a) and using the relation (2c):

$$\boldsymbol{\alpha}_{21}\mathbf{F}_{S1} + \boldsymbol{\alpha}_{22}\mathbf{F}_{S2} = \boldsymbol{\beta}_{22}\mathbf{F}_{P2} + \boldsymbol{\beta}_{23}\mathbf{F}_{P3}, \tag{3a}$$

$$\mathbf{F}_{P2} = [\boldsymbol{\alpha}_{22} + \boldsymbol{\beta}_{22}]^{-1}[\boldsymbol{\alpha}_{21}\mathbf{F}_{S1} - \boldsymbol{\beta}_{23}\mathbf{F}_{P3}]. \tag{3b}$$

Similarly, internal forces at location 3 are derived by using equations (1d), (1e) and (2b) along with equation (2d):

$$\boldsymbol{\beta}_{32}\mathbf{F}_{P2} + \boldsymbol{\beta}_{33}\mathbf{F}_{P3} = \boldsymbol{\gamma}_{33}\mathbf{F}_{R3} + \boldsymbol{\gamma}_{34}\mathbf{F}_{R4}, \tag{4a}$$

$$\mathbf{F}_{R3} = [\boldsymbol{\beta}_{33} + \boldsymbol{\gamma}_{33}]^{-1}[\boldsymbol{\beta}_{32}\mathbf{F}_{P2} - \boldsymbol{\gamma}_{34}\mathbf{F}_{R4}]. \tag{4b}$$

Substituting equation (3b) into equation (4b) and using equation (2d) lead to the following interfacial forces at location 3 when external forces are applied at locations 1 (source) and 4 (receiver):

$$\begin{aligned}\mathbf{F}_{R3} = {} & [[\boldsymbol{\beta}_{33} + \boldsymbol{\gamma}_{33}] - \boldsymbol{\beta}_{32}[\boldsymbol{\alpha}_{22} + \boldsymbol{\beta}_{22}]^{-1}\boldsymbol{\beta}_{23}]^{-1}\,\boldsymbol{\beta}_{32}[\boldsymbol{\alpha}_{22} + \boldsymbol{\beta}_{22}]^{-1}\boldsymbol{\alpha}_{21}\mathbf{F}_{S1} \\ & - [[\boldsymbol{\beta}_{33} + \boldsymbol{\gamma}_{33}] - \boldsymbol{\beta}_{32}\,[\boldsymbol{\alpha}_{22} + \boldsymbol{\beta}_{22}]^{-1}\boldsymbol{\beta}_{23}]^{-1}\boldsymbol{\gamma}_{34}\,\mathbf{F}_{R4}.\end{aligned} \tag{5}$$

Similarly, internal forces between source (S) and path (P) are obtained by substituting equation (4b) into equation (3b) and using equation (2d):

$$\begin{aligned}\mathbf{F}_{P2} = {} & [[\boldsymbol{\alpha}_{22} + \boldsymbol{\beta}_{22}] - \boldsymbol{\beta}_{23}\,[\boldsymbol{\beta}_{33} + \boldsymbol{\gamma}_{33}]^{-1}\boldsymbol{\beta}_{32}]^{-1}\boldsymbol{\alpha}_{21}\mathbf{F}_{S1} \\ & - [[\boldsymbol{\alpha}_{22} + \boldsymbol{\beta}_{22}] - \boldsymbol{\beta}_{23}\,[\boldsymbol{\beta}_{33} + \boldsymbol{\gamma}_{33}]^{-1}\boldsymbol{\beta}_{32}]^{-1}\,\boldsymbol{\beta}_{23}\,[\boldsymbol{\beta}_{33} + \boldsymbol{\gamma}_{33}]^{-1}\boldsymbol{\gamma}_{34}\,\mathbf{F}_{R4}.\end{aligned} \tag{6}$$

From equations (5) and (6), each interfacial force can be expressed as follows when location 4 at the receiver is free:

$$\mathbf{F}_{P2} = [[\boldsymbol{\alpha}_{22} + \boldsymbol{\beta}_{22}] - \boldsymbol{\beta}_{23}[\boldsymbol{\beta}_{33} + \boldsymbol{\gamma}_{33}]^{-1}\boldsymbol{\beta}_{32}]^{-1}\boldsymbol{\alpha}_{21}\mathbf{F}_{S1}, \tag{7a}$$

$$\mathbf{F}_{R3} = [[\boldsymbol{\beta}_{33} + \boldsymbol{\gamma}_{33}] - \boldsymbol{\beta}_{32}[\boldsymbol{\alpha}_{22} + \boldsymbol{\beta}_{22}]^{-1}\boldsymbol{\beta}_{23}]^{-1}\boldsymbol{\beta}_{32}[\boldsymbol{\alpha}_{22} + \boldsymbol{\beta}_{22}]^{-1}\boldsymbol{\alpha}_{21}\mathbf{F}_{S1}. \tag{7b}$$

Also, when location 1 at the source is free, the interfacial forces are

$$\mathbf{F}_{P2} = -[[\boldsymbol{\alpha}_{22} + \boldsymbol{\beta}_{22}] - \boldsymbol{\beta}_{23}[\boldsymbol{\beta}_{33} + \boldsymbol{\gamma}_{33}]^{-1}\boldsymbol{\beta}_{32}]^{-1}\boldsymbol{\beta}_{23}[\boldsymbol{\beta}_{33} + \boldsymbol{\gamma}_{33}]^{-1}\boldsymbol{\gamma}_{34}\mathbf{F}_{R4}, \tag{7c}$$

$$\mathbf{F}_{R3} = -[[\boldsymbol{\beta}_{33} + \boldsymbol{\gamma}_{33}] - \boldsymbol{\beta}_{32}[\boldsymbol{\alpha}_{22} + \boldsymbol{\beta}_{22}]^{-1}\boldsymbol{\beta}_{23}]^{-1}\boldsymbol{\gamma}_{34}\mathbf{F}_{R4}. \tag{7d}$$

Next, the mobilities ($\mathbf{M}_{ij}$) of the synthesized system are represented in terms of mobilities of components $\boldsymbol{\alpha}_{ij}$, $\boldsymbol{\beta}_{ij}$ and $\boldsymbol{\gamma}_{ij}$, where $\mathbf{V}_1 = \mathbf{M}_{11}\mathbf{F}_{S1}$, $\mathbf{V}_1 = \mathbf{M}_{14}\mathbf{F}_{R4}$, $\mathbf{V}_4 = \mathbf{M}_{41}\mathbf{F}_{S1}$ and $\mathbf{V}_4 = \mathbf{M}_{44}\mathbf{F}_{R4}$, by using the interfacial forces derived above in equations (7a–d), (1a) and (1f). First, consider mobility matrix $\mathbf{M}_{11}$. Substituting $\mathbf{F}_{S2}$ that is obtained by combining equations (7a) and (2c) into equation (1a) yields velocity at location 1 when an external force is applied at 1 (source):

$$\mathbf{M}_{11} = \boldsymbol{\alpha}_{11} + \boldsymbol{\alpha}_{12}[\boldsymbol{\beta}_{23}[\boldsymbol{\beta}_{33} + \boldsymbol{\gamma}_{33}]^{-1}\boldsymbol{\beta}_{32} - [\boldsymbol{\alpha}_{22} + \boldsymbol{\beta}_{22}]]^{-1}\boldsymbol{\alpha}_{21}. \tag{8a}$$

Also, the velocity at location 4 with force application only at location 1 is found by substituting equation (7b) into equation (1f) and letting $\mathbf{F}_{R4} = 0$:

$$\mathbf{M}_{41} = -\boldsymbol{\gamma}_{43}[\boldsymbol{\beta}_{32}[\boldsymbol{\alpha}_{22} + \boldsymbol{\beta}_{22}]^{-1}\boldsymbol{\beta}_{23} - [\boldsymbol{\beta}_{33} + \boldsymbol{\gamma}_{33}]]^{-1}\boldsymbol{\beta}_{32}[\boldsymbol{\alpha}_{22} + \boldsymbol{\beta}_{22}]^{-1}\boldsymbol{\alpha}_{21}. \tag{8b}$$

In a similar fashion, velocities at ends (1 and 4) when a force is applied only at 4 can be obtained from the following:

$$\mathbf{M}_{14} = -\boldsymbol{\alpha}_{12}[\boldsymbol{\beta}_{23}[\boldsymbol{\beta}_{33} + \boldsymbol{\gamma}_{33}]^{-1}\boldsymbol{\beta}_{32} - [\boldsymbol{\alpha}_{22} + \boldsymbol{\beta}_{22}]]^{-1}\boldsymbol{\beta}_{23}[\boldsymbol{\beta}_{33} + \boldsymbol{\gamma}_{33}]^{-1}\boldsymbol{\gamma}_{34}, \tag{8c}$$

$$\mathbf{M}_{44} = \boldsymbol{\gamma}_{44} + \boldsymbol{\gamma}_{43}[\boldsymbol{\beta}_{32}[\boldsymbol{\alpha}_{22} + \boldsymbol{\beta}_{22}]^{-1}\boldsymbol{\beta}_{23} - [\boldsymbol{\beta}_{33} + \boldsymbol{\gamma}_{33}]]^{-1}\boldsymbol{\gamma}_{34}. \tag{8d}$$

In addition, velocities at intermediate locations can be derived by using a similar procedure. Substituting $\mathbf{F}_{S2}$, obtained by combining equations (7a) and (2c) into equation (1b) yields the velocity at location 2 when an external force is applied at 1:

$$\mathbf{V}_2 = \mathbf{M}_{21}\mathbf{F}_{S1} = [\boldsymbol{\alpha}_{21} - \boldsymbol{\alpha}_{22}[[\boldsymbol{\alpha}_{22} + \boldsymbol{\beta}_{22}] - \boldsymbol{\beta}_{23}[\boldsymbol{\beta}_{33} + \boldsymbol{\gamma}_{33}]^{-1}\boldsymbol{\beta}_{32}]^{-1}\boldsymbol{\alpha}_{21}]\,\mathbf{F}_{S1}. \tag{9a}$$

Also, the velocity at location 3 for a force application at 1 is derived as follows by using equations (7b) and (1e) and letting $\mathbf{F}_{R4} = 0$:

$$\mathbf{V}_3 = \mathbf{M}_{31}\mathbf{F}_{S1} = \boldsymbol{\gamma}_{33}[[\boldsymbol{\beta}_{33} + \boldsymbol{\gamma}_{33}] - \boldsymbol{\beta}_{32}[\boldsymbol{\alpha}_{22} + \boldsymbol{\beta}_{22}]^{-1}\boldsymbol{\beta}_{23}]^{-1}\boldsymbol{\beta}_{32}[\boldsymbol{\alpha}_{22} + \boldsymbol{\beta}_{22}]^{-1}\boldsymbol{\alpha}_{21}\,\mathbf{F}_{S1}. \tag{9b}$$

Similarly, velocities at an intermediate location when the force is applied only at 4 can be obtained as follows:

$$\mathbf{V}_2 = \mathbf{M}_{24}\mathbf{F}_{R4} = \boldsymbol{\alpha}_{22}[[\boldsymbol{\alpha}_{22} + \boldsymbol{\beta}_{22}] - \boldsymbol{\beta}_{23}[\boldsymbol{\beta}_{33} + \boldsymbol{\gamma}_{33}]^{-1}\boldsymbol{\beta}_{32}]^{-1}\boldsymbol{\beta}_{23}[\boldsymbol{\beta}_{33} + \boldsymbol{\gamma}_{33}]^{-1}\boldsymbol{\gamma}_{34}\,\mathbf{F}_{R4}, \tag{9c}$$

$$\mathbf{V}_3 = \mathbf{M}_{34}\mathbf{F}_{R4} = [\boldsymbol{\gamma}_{34} - \boldsymbol{\gamma}_{33}[[\boldsymbol{\beta}_{33} + \boldsymbol{\gamma}_{33}] - \boldsymbol{\beta}_{32}[\boldsymbol{\alpha}_{22} + \boldsymbol{\beta}_{22}]^{-1}\boldsymbol{\beta}_{23}]^{-1}\boldsymbol{\gamma}_{34}\,\mathbf{F}_{R4}. \tag{9d}$$

4.2. DECOMPOSITION OF COMPONENT MOBILITIES

Let us assume that an isolator acts as a path in Figure 1(b). Its mobility $\boldsymbol{\beta}_{ij}$ for $i, j = 2, 3$ is defined by (8a–d) where $\mathbf{V}_{P2} = \boldsymbol{\beta}_{22}\mathbf{F}_{P2}$, $\mathbf{V}_{P2} = \boldsymbol{\beta}_{23}\mathbf{F}_{P3}$, $\mathbf{V}_{P3} = \boldsymbol{\beta}_{32}\mathbf{F}_{P2}$ and $\mathbf{V}_{P3} = \boldsymbol{\beta}_{33}\mathbf{F}_{P3}$. Therefore, we need to extract four unknowns $\boldsymbol{\beta}_{22}$, $\boldsymbol{\beta}_{23}$, $\boldsymbol{\beta}_{32}$ and $\boldsymbol{\beta}_{33}$ from the mobility equations (8a–d) of the combined system.

First, rewrite equations (8a) and (8c) as follows:

$$\boldsymbol{\beta}_{23}[\boldsymbol{\beta}_{33} + \boldsymbol{\gamma}_{33}]^{-1}\boldsymbol{\beta}_{32} - [\boldsymbol{\alpha}_{22} + \boldsymbol{\beta}_{22}] = \boldsymbol{\alpha}_{21}[\mathbf{M}_{11} - \boldsymbol{\alpha}_{11}]^{-1}\boldsymbol{\alpha}_{12}. \tag{10a}$$

$$\boldsymbol{\beta}_{23}[\boldsymbol{\beta}_{33} + \boldsymbol{\gamma}_{33}]^{-1}\boldsymbol{\beta}_{32} - [\boldsymbol{\alpha}_{22} + \boldsymbol{\beta}_{22}] = -\boldsymbol{\beta}_{23}[\boldsymbol{\beta}_{33} + \boldsymbol{\gamma}_{33}]^{-1}\boldsymbol{\gamma}_{34}\mathbf{M}_{14}^{-1}\boldsymbol{\alpha}_{12}, \tag{10b}$$

Equating equations (10a) and (10b) leads to the equation

$$[\boldsymbol{\beta}_{33} + \boldsymbol{\gamma}_{33}]\boldsymbol{\beta}_{23}^{-1}\boldsymbol{\alpha}_{21}[\mathbf{M}_{11} - \boldsymbol{\alpha}_{11}]^{-1}\boldsymbol{\alpha}_{12} = -\boldsymbol{\gamma}_{34}\mathbf{M}_{14}^{-1}\boldsymbol{\alpha}_{12}. \tag{11}$$

Next, rewrite equations (8b) and (8d) as

$$\boldsymbol{\beta}_{32}[\boldsymbol{\alpha}_{22} + \boldsymbol{\beta}_{22}]^{-1}\boldsymbol{\beta}_{23} - [\boldsymbol{\beta}_{33} + \boldsymbol{\gamma}_{33}] = -\boldsymbol{\beta}_{32}[\boldsymbol{\alpha}_{22} + \boldsymbol{\beta}_{22}]^{-1}\boldsymbol{\alpha}_{21}\mathbf{M}_{41}^{-1}\boldsymbol{\gamma}_{43}, \tag{12a}$$

$$\boldsymbol{\beta}_{32}[\boldsymbol{\alpha}_{22} + \boldsymbol{\beta}_{22}]^{-1}\boldsymbol{\beta}_{23} - [\boldsymbol{\beta}_{33} + \boldsymbol{\gamma}_{33}] = \boldsymbol{\gamma}_{34}[\mathbf{M}_{44} - \boldsymbol{\gamma}_{44}]^{-1}\boldsymbol{\gamma}_{43}. \tag{12b}$$

Solving equations (12a) and (12b) simultaneously in terms of $[\boldsymbol{\beta}_{33} + \boldsymbol{\gamma}_{33}]$ yields the following:

$$-[\boldsymbol{\beta}_{33} + \boldsymbol{\gamma}_{33}][\boldsymbol{\beta}_{32} + \boldsymbol{\alpha}_{21}\mathbf{M}_{41}^{-1}\boldsymbol{\gamma}_{43}]^{-1}\boldsymbol{\alpha}_{21}\mathbf{M}_{41}^{-1}\boldsymbol{\gamma}_{43} = \boldsymbol{\gamma}_{34}[\mathbf{M}_{44} - \boldsymbol{\gamma}_{44}]^{-1}\boldsymbol{\gamma}_{43}. \tag{13}$$

Further, simplify the above equation (13) as follows:

$$[\boldsymbol{\beta}_{33} + \boldsymbol{\gamma}_{33}] = -\boldsymbol{\gamma}_{34}[\mathbf{M}_{44} - \boldsymbol{\gamma}_{44}]^{-1}[\mathbf{M}_{41}\boldsymbol{\alpha}_{21}^{-1} + \boldsymbol{\gamma}_{43}\boldsymbol{\beta}_{23}^{-1}]\boldsymbol{\beta}_{23}. \tag{14}$$

Substituting equation (14) into equation (11) and simplifying the resulting equation yields

$$[\mathbf{M}_{41}\boldsymbol{\alpha}_{21}^{-1} + \boldsymbol{\gamma}_{43}\boldsymbol{\beta}_{23}^{-1}] = [\mathbf{M}_{44} - \boldsymbol{\gamma}_{44}]\mathbf{M}_{14}^{-1}[\mathbf{M}_{11} - \boldsymbol{\alpha}_{11}]\boldsymbol{\alpha}_{21}^{-1}. \tag{15}$$

Finally, the transfer mobility matrix of isolator $\boldsymbol{\beta}_{23}$ is obtained as follows from equation (15):

$$\boldsymbol{\beta}_{23} = \boldsymbol{\alpha}_{21}[[\mathbf{M}_{44} - \boldsymbol{\gamma}_{44}]\mathbf{M}_{14}^{-1}[\mathbf{M}_{11} - \boldsymbol{\alpha}_{11}] - \mathbf{M}_{41}]^{-1}\boldsymbol{\gamma}_{43}. \tag{16}$$

Also, substituting equation (16) into equation (11) yields the driving point mobility matrix $\boldsymbol{\beta}_{33}$:

$$\boldsymbol{\beta}_{33} = -\boldsymbol{\gamma}_{33} - \boldsymbol{\gamma}_{34}\mathbf{M}_{14}^{-1}[\mathbf{M}_{11} - \boldsymbol{\alpha}_{11}][[\mathbf{M}_{44} - \boldsymbol{\gamma}_{44}]\mathbf{M}_{14}^{-1}[\mathbf{M}_{11} - \boldsymbol{\alpha}_{11}] - \mathbf{M}_{41}]^{-1}\boldsymbol{\gamma}_{43}. \tag{17}$$

Next, consider $\boldsymbol{\beta}_{22}$ and $\boldsymbol{\beta}_{32}$. Analogous to the previous derivation, solving equations (12a) and (12b) simultaneously in terms of $[\boldsymbol{\alpha}_{22} + \boldsymbol{\beta}_{22}]$ yields

$$[\boldsymbol{\alpha}_{22} + \boldsymbol{\beta}_{22}]\boldsymbol{\beta}_{32}^{-1}\boldsymbol{\gamma}_{34}[\mathbf{M}_{44} - \boldsymbol{\gamma}_{44}]^{-1}\boldsymbol{\gamma}_{43} = -\boldsymbol{\alpha}_{21}\mathbf{M}_{41}^{-1}\boldsymbol{\gamma}_{43}. \tag{18}$$

Similarly, equations (10a) and (10b) are simultaneously solved in terms of $[\boldsymbol{\alpha}_{22} + \boldsymbol{\beta}_{22}]$:

$$-[\boldsymbol{\alpha}_{22} + \boldsymbol{\beta}_{22}][\boldsymbol{\beta}_{32} + \boldsymbol{\gamma}_{34}\mathbf{M}_{14}^{-1}\boldsymbol{\alpha}_{12}]^{-1}\boldsymbol{\gamma}_{34}\mathbf{M}_{14}^{-1}\boldsymbol{\alpha}_{12} = \boldsymbol{\alpha}_{21}[\mathbf{M}_{11} - \boldsymbol{\alpha}_{11}]^{-1}\boldsymbol{\alpha}_{12}. \tag{19}$$

The above equation is rewritten as follows:

$$[\boldsymbol{\alpha}_{22} + \boldsymbol{\beta}_{22}] = -\boldsymbol{\alpha}_{21}[\mathbf{M}_{11} - \boldsymbol{\alpha}_{11}]^{-1}[\mathbf{M}_{14}\boldsymbol{\gamma}_{34}^{-1} + \boldsymbol{\alpha}_{12}\boldsymbol{\beta}_{32}^{-1}]\boldsymbol{\beta}_{32}. \tag{20}$$

Substitution of equation (20) into equation (18) yields

$$[\mathbf{M}_{14}\boldsymbol{\gamma}_{34}^{-1} + \boldsymbol{\alpha}_{12}\boldsymbol{\beta}_{32}^{-1}] = [\mathbf{M}_{11} - \boldsymbol{\alpha}_{11}]\mathbf{M}_{41}^{-1}[\mathbf{M}_{44} - \boldsymbol{\gamma}_{44}]\boldsymbol{\gamma}_{34}^{-1}. \tag{21}$$

Finally, $\boldsymbol{\beta}_{32}$ is obtained from equation (21) as follows:

$$\boldsymbol{\beta}_{32} = \boldsymbol{\gamma}_{34}[[\mathbf{M}_{11} - \boldsymbol{\alpha}_{11}]\mathbf{M}_{41}^{-1}[\mathbf{M}_{44} - \boldsymbol{\gamma}_{44}] - \mathbf{M}_{14}]\boldsymbol{\alpha}_{12}. \tag{22}$$

Additionally, the driving point mobility, $\boldsymbol{\beta}_{22}$ is derived by substituting equation (22) into equation (18):

$$\boldsymbol{\beta}_{22} = -\boldsymbol{\alpha}_{22} - \boldsymbol{\alpha}_{21}\mathbf{M}_{41}^{-1}[\mathbf{M}_{44} - \boldsymbol{\gamma}_{44}][[\mathbf{M}_{11} - \boldsymbol{\alpha}_{11}]\ \mathbf{M}_{41}^{-1}[\mathbf{M}_{44} - \boldsymbol{\gamma}_{44}] - \mathbf{M}_{14}]^{-1}\boldsymbol{\alpha}_{12}. \tag{23}$$

Driving point mobilities (17) and (23) are further simplified to yield

$$\boldsymbol{\beta}_{22} = -\boldsymbol{\alpha}_{22} - \boldsymbol{\alpha}_{21}[[\mathbf{M}_{11} - \boldsymbol{\alpha}_{11}] - \mathbf{M}_{14}[\mathbf{M}_{44} - \boldsymbol{\gamma}_{44}]^{-1}\mathbf{M}_{41}]^{-1}\ \boldsymbol{\alpha}_{12}, \tag{24}$$

$$\boldsymbol{\beta}_{33} = -\boldsymbol{\gamma}_{33} - \boldsymbol{\gamma}_{34}[[\mathbf{M}_{44} - \boldsymbol{\gamma}_{44}] - \mathbf{M}_{41}[\mathbf{M}_{11} - \boldsymbol{\alpha}_{11}]^{-1}\mathbf{M}_{14}]^{-1}\boldsymbol{\gamma}_{43}. \tag{25}$$

5. SIMULATION EXAMPLE FOR MOBILITY SYNTHESIS AND DECOMPOSITION

5.1. PHYSICAL SYSTEM

Figure 2(b) shows a simulation example that consists of an elastic beam and two rigid masses where EI_S is the flexural rigidity of the beam and I_m is the moment of inertia corresponding to lumped masses (m_a and m_b). Here, f and q are harmonic force and moment excitation amplitudes, respectively, at frequency ω, and subscripts a, b and G represent mass a, mass b and mass center respectively. Mobilities of the combined system are obtained from the mobility synthesis formulation using equations (8a–d) and compared with the direct analytical solution that follows.

5.2. DIRECT ANALYTICAL METHOD

Harmonic responses of a beam are derived for both longitudinal (X) and flexural (Y) motions where k is the wave number of the beam, and A, B, C and D are arbitrary constants. Subscripts L and B are used to denote longitudinal and bending motions of the beam, respectively:

$$X(x, t) = X(x)\,\mathrm{e}^{\mathrm{j}\omega t} = \{A_L \sin[k_L x] + B_L \cos[k_L x]\}\,\mathrm{e}^{\mathrm{j}\omega t}, \tag{26a}$$

$$Y(x, t) = Y(x)\,\mathrm{e}^{\mathrm{j}\omega t} = \{A_B \sin[k_B x] + B_B \cos[k_B x] + C_B \sinh[k_B x] + D_B \cosh[k_B x]\}\,\mathrm{e}^{\mathrm{j}\omega t}. \tag{26b}$$

The governing equations in the frequency domain are described as follows where the ubiquitous term $\mathrm{e}^{\mathrm{j}\omega t}$ is dropped:

$$-m_a\omega^2 X(0) - SE\frac{\mathrm{d}X(0)}{\mathrm{d}x} = f_{xa}, \tag{27a}$$

$$-m_a\omega^2 Y(0) + m_a h_a\omega^2\frac{\mathrm{d}Y(0)}{\mathrm{d}x} + EI_S\frac{\mathrm{d}^3 Y(0)}{\mathrm{d}x^3} = f_{ya}, \tag{27b}$$

$$-(I_{amG}+m_a h_a^2)\omega^2\frac{\mathrm{d}Y(0)}{\mathrm{d}x}+m_a\omega^2 Y(0)-EI_S\frac{\mathrm{d}^2Y(0)}{\mathrm{d}x^2}=q_a, \tag{27c}$$

$$-m_a\omega^2 X(L)+SE\frac{\mathrm{d}X(L)}{\mathrm{d}x}=f_{xb}, \tag{27d}$$

$$-m_b\omega^2 Y(L)-m_b h_b\omega^2\frac{\mathrm{d}Y(L)}{\mathrm{d}x}-EI_S\frac{\mathrm{d}^3Y(L)}{\mathrm{d}x^3}=f_{yb} \tag{27e}$$

$$-(I_{bmG}+m_b h_b^2)\omega^2\frac{\mathrm{d}Y(L)}{\mathrm{d}x}-m_b\omega^2 Y(L)+EI_S\frac{\mathrm{d}^2Y(L)}{\mathrm{d}x^2}=q_b \tag{27f}$$

When the harmonic force f is applied at location 1 of mass a, $f_a=f$, $q_a=-2h_a f$ and $f_b=q_b=0$ and when the force excitation f is shifted to location 4 of mass b, $f_b=f$, $q_b=2h_b f$ and $f_a=q_a=0$. Also, $f_a=0$, $q_a=q$ and $f_b=q_b=0$ when a harmonic moment q is applied at location 1 of mass a, and $f_b=0$, $q_b=q$ and $f_a=q_a=0$ for the moment excitation q at location 4 of mass b. Therefore, harmonic flexural motions, $Y(x)$ and $\mathrm{d}Y(x)/\mathrm{d}x$ for each excitation, are separately obtained by solving the boundary conditions (27a–f) in terms of arbitrary constants A_B, B_B, C_B and D_B. Also, the translational and rotational velocities at locations 1 and 4 are related to the flexural displacements and slopes at connections 1 and 4 as follows:

$$v_1=\mathrm{j}\omega\left[Y(0)-2h_a\frac{\mathrm{d}Y(0)}{\mathrm{d}x}\right],\qquad \frac{\mathrm{d}v_1}{\mathrm{d}x}=\mathrm{j}\omega\frac{\mathrm{d}Y(0)}{\mathrm{d}x}, \tag{28a, b}$$

$$v_4=\mathrm{j}\omega\left[Y(L)+2h_b\frac{\mathrm{d}Y(L)}{\mathrm{d}x}\right],\qquad \frac{\mathrm{d}v_4}{\mathrm{d}x}=\mathrm{j}\omega\frac{\mathrm{d}Y(L)}{\mathrm{d}x}. \tag{28c, d}$$

5.3. MOBILITY MATRIX OF A RIGID BODY

Assume that the source of Figure 1(a) is a rigid body like the example of Figure 2(a). Now we determine the mobility matrix that characterizes the relationship between multi-dimensional excitations at frequency ω and the steady state velocity responses through the rigid mass (m). First, the mobility matrix $\mathbf{M}(\omega)$ is defined in terms of velocity vector $\mathbf{V}_G$ at the mass center (G), $\mathbf{V}_G=\mathbf{M}_{GG}\mathbf{F}_G$, where $\mathbf{F}_G$ is the excitation vector. Decompose the formulation in terms of translational ($\mathbf{v}$) and rotational ($\mathbf{w}$) components, and define

$$\mathbf{M}_{GG}=\begin{bmatrix}\mathbf{M}_{v,GG} & 0\\ 0 & \mathbf{M}_{w,GG}\end{bmatrix}, \tag{29a}$$

$$\mathbf{M}_{v,GG}=\mathrm{diag}\left(\begin{bmatrix}\frac{1}{m\mathrm{j}\omega} & \frac{1}{m\mathrm{j}\omega} & \frac{1}{m\mathrm{j}\omega}\end{bmatrix}\right),\qquad \mathbf{M}_{w,GG}=\frac{1}{\mathrm{j}\omega}\begin{bmatrix}I_{m,xx} & -I_{m,xy} & -I_{m,xz}\\ -I_{m,xy} & I_{m,yy} & -I_{m,yz}\\ -I_{m,xz} & -I_{m,yz} & I_{m,zz}\end{bmatrix}^{-1}, \tag{29b, c}$$

$$\mathbf{V}_G=\begin{bmatrix}\mathbf{v}_G\\ \mathbf{w}_G\end{bmatrix},\qquad \mathbf{F}_G=\begin{bmatrix}\mathbf{f}_G\\ \mathbf{q}_G\end{bmatrix}. \tag{29d, e}$$

Next, the mobility matrix at an arbitrary location (i) is obtained by relating $\mathbf{V}$ and $\mathbf{F}$ at i with corresponding vectors at G where $\mathbf{r}_{iG}$ is the position vector from G to reference point i:

$$\mathbf{V}_i = \begin{bmatrix} \mathbf{v}_G \\ \mathbf{w}_G \end{bmatrix} + \begin{bmatrix} \mathbf{w}_G \times \mathbf{r}_{iG} \\ 0 \end{bmatrix}, \qquad \mathbf{F}_i = \begin{bmatrix} \mathbf{f}_G \\ \mathbf{q}_G \end{bmatrix} - \begin{bmatrix} 0 \\ \mathbf{r}_{iG} \times \mathbf{f}_G \end{bmatrix}. \tag{30a, b}$$

For the sake of convenience, the following transformation matrix $\mathbf{T}_i$ is defined in conjunction with a rotation matrix $\mathbf{R}_i$ to represent the above expressions where h_{xi}, h_{yi} and h_{zi} are the components of the position vector $\mathbf{r}_{iG}$:

$$\mathbf{T}_i = \begin{bmatrix} \mathbf{I} & 0 \\ \mathbf{R}_i & \mathbf{I} \end{bmatrix}, \qquad \mathbf{R}_i = \begin{bmatrix} 0 & -h_{zi} & h_{yi} \\ h_{zi} & 0 & -h_{xi} \\ -h_{yi} & h_{xi} & 0 \end{bmatrix}. \tag{31a, b}$$

Using equations (30) and (31), $\mathbf{V}_i$ and $\mathbf{F}_i$ are described as

$$\mathbf{V}_i = \begin{bmatrix} \mathbf{I} & \mathbf{R}_i^{\mathrm{T}} \\ 0 & \mathbf{I} \end{bmatrix} \begin{bmatrix} \mathbf{v}_G \\ \mathbf{w}_G \end{bmatrix} = \mathbf{T}_i^{\mathrm{T}} \mathbf{V}_G, \qquad \mathbf{F}_i = \begin{bmatrix} \mathbf{I} & 0 \\ -\mathbf{R}_i & \mathbf{I} \end{bmatrix} \begin{bmatrix} \mathbf{f}_G \\ \mathbf{q}_G \end{bmatrix} = \mathbf{T}_i^{-1} \mathbf{F}_G. \tag{32a, b}$$

Using the relationships $\mathbf{V}_G = \mathbf{M}_{GG}\mathbf{F}_G$, $\mathbf{V}_G = [\mathbf{T}_i^{\mathrm{T}}]^{-1}\mathbf{V}_i$ and $\mathbf{F}_G = \mathbf{T}_i\mathbf{F}_i$, each mobility matrix at point i can be obtained. The relation $\mathbf{V}_G = \mathbf{M}_{GG}\mathbf{T}_i\mathbf{F}_i$ and the definition $\mathbf{V}_G = \mathbf{M}_{Gi}\mathbf{F}_i$ lead to the mobility equation $\mathbf{M}_{Gi} = \mathbf{M}_{GG}\mathbf{T}_i$. Similarly, define $\mathbf{M}_{iG} = \mathbf{T}_i^{\mathrm{T}}\mathbf{M}_{GG}$, $\mathbf{V}_i = \mathbf{M}_{iG}\mathbf{F}_G$ and $\mathbf{V}_i = \mathbf{T}_i^{\mathrm{T}}\mathbf{V}_G$. Also, the driving point mobility $\mathbf{M}_{ii} = \mathbf{T}_i^{\mathrm{T}}\mathbf{M}_{GG}\mathbf{T}_i$ can be obtained from the relations $\mathbf{V}_i = \mathbf{M}_{ii}\mathbf{F}_i = \mathbf{M}_{ii}\mathbf{T}_i^{-1}\mathbf{F}_G$ and $\mathbf{V}_i = \mathbf{T}_i^{\mathrm{T}}\mathbf{V}_G = \mathbf{T}_i^{\mathrm{T}}\mathbf{M}_{GG}\mathbf{F}_G$. In a similar manner, the transfer mobility $\mathbf{M}_{ij} = \mathbf{T}_i^{\mathrm{T}}\mathbf{M}_{GG}\mathbf{T}_j$ between two points (say i and j) other than the mass center can be determined from the relations $\mathbf{V}_i = \mathbf{M}_{ij}\mathbf{F}_j = \mathbf{T}_i^{\mathrm{T}}\mathbf{M}_{GG}\mathbf{F}_G$ and $\mathbf{F}_j = \mathbf{T}_j^{-1}\mathbf{F}_G$. The transfer mobility $\mathbf{M}_{ji}$ can be obtained in the same way and the reciprocity relation $\mathbf{M}_{ij} = \mathbf{M}_{ji}^{\mathrm{T}}$ is satisfied. Therefore, the mobility matrix of a rigid body, between any two points i and j, can be determined from the inertia properties (G) and geometry information. The mobility matrix $\mathbf{M}_{GG}$ is summarized as follows where it should be noted that the small angle (θ) approximation ($\sin\theta \approx \tan\theta \approx \theta$ and $\cos\theta \approx 1$) has been applied throughout:

$$\begin{bmatrix} \mathbf{V}_i \\ \mathbf{V}_j \end{bmatrix} = \begin{bmatrix} \mathbf{M}_{ii} & \mathbf{M}_{ij} \\ \mathbf{M}_{ji} & \mathbf{M}_{jj} \end{bmatrix} \begin{bmatrix} \mathbf{F}_i \\ \mathbf{F}_j \end{bmatrix} = \begin{bmatrix} \mathbf{T}_i^{\mathrm{T}}\mathbf{M}_{GG}\mathbf{T}_i & \mathbf{T}_i^{\mathrm{T}}\mathbf{M}_{GG}\mathbf{T}_j \\ \mathbf{T}_j^{\mathrm{T}}\mathbf{M}_{GG}\mathbf{T}_i & \mathbf{T}_j^{\mathrm{T}}\mathbf{M}_{GG}\mathbf{T}_j \end{bmatrix} \begin{bmatrix} \mathbf{F}_i \\ \mathbf{F}_j \end{bmatrix}. \tag{33}$$

5.4. COMPARISON OF TWO METHODS

The calculations are performed using both procedures for a circular beam with modulus of elasticity (E) of 8×10^5 N/m^2, mass density (ρ) of 1000 kg/m^3 and a loss factor (η) of 0·1. The radius and length of the beam are 12 and 30 mm respectively. Masses of rigid bodies a and b are 0·65 and 0·55 kg, respectively, and the corresponding dimensions in x, y and z directions are 75, 50 and 64 mm for mass a and 68, 50 and 50 mm for mass b. Mobilities of the combined system are calculated by employing the mobility synthesis formulation (8a–d) based on the base driven beam mobilities and the mobilities of rigid bodies a and b.

Given the input parameters, mobilities at locations 1 and 4 of the combined system may be obtained. Predictions via the mobility synthesis formulation (8a–d) are compared with the direct analytical solution in Figures 5 and 7. Also, the mobilities of the beam are extracted from the results of the combined system using equations (16, 17) and (24, 25) and

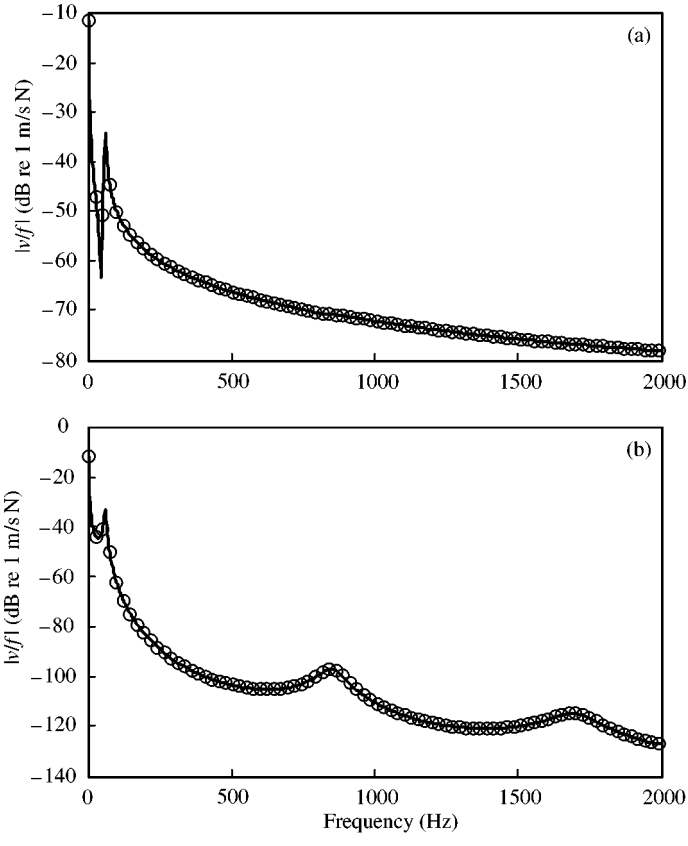

Figure 5. Synthesized mobilities for a system consisting of two rigid masses and an elastic beam in longitudinal motion as shown in Figure 2(b). (a) driving point mobility; (b) transfer mobility. Key: ————, synthesized or decomposed mobility; ○, direct analytical solution.

then compared with the analytical mobilities of the beam. As evident from the results of Figures 6 and 8, both methods yield the same answers. Only the proposed mobility method will be used in further studies.

6. EXAMINATION OF APPROXIMATE METHODS

6.1. FORMULATION

Several attempts have been made for the identification of transfer stiffnesses including the rotational component [10–13]. Such schemes typically consider a resilient element that is located between two inertial components as shown in Figure 9. The first method focuses on high-frequency properties [10, 11] and it may be applied to either axial or flexural motions. The second method improves the axial (compressional) stiffness at low frequencies by modifying the first scheme [12, 13]. In our study, key procedures of such approximate methods are briefly explained, using the mobility method for the sake of consistency. Both approximate schemes are analytically examined using a simulation example. Further, the second approximate method is extended to the identification of flexural stiffnesses.

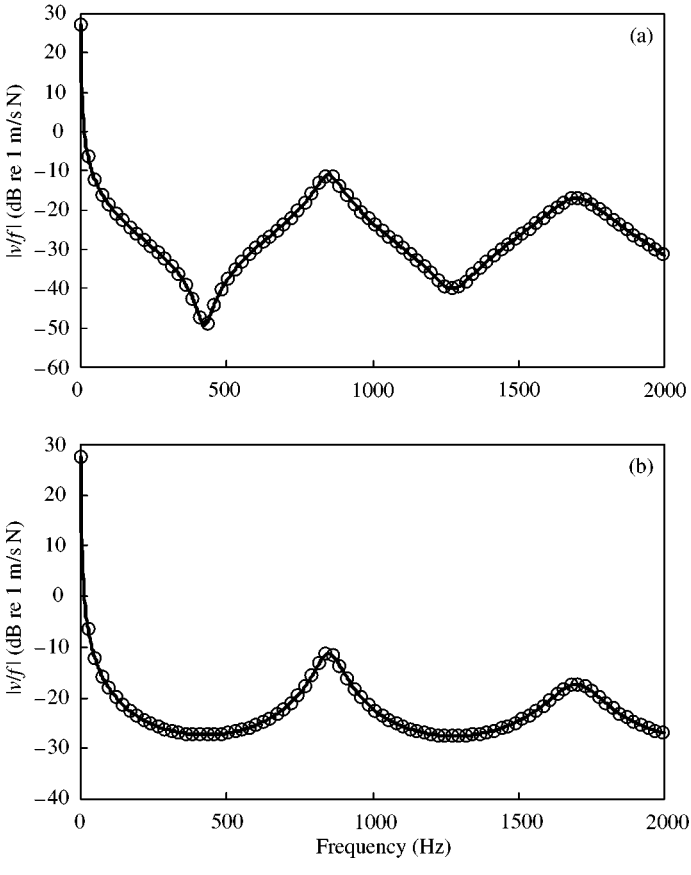

Figure 6. Decomposed mobilities for a beam using a system consisting of two rigid masses and an elastic beam as shown in Figure 2(b): (a) driving point mobility; (d) transfer mobility. Key: ———, decomposed mobility; ○, direct analytical solution.

6.2. APPROXIMATE METHOD FOR AXIAL MOTIONS

The discrete system of Figure 9 is examined using the mobility method. This obviously yields the results reported by Thompson *et al.* [12] based on lumped system theory. Here, β_{22} and β_{33} are the driving point mobilities of the isolator, β_{23} and β_{32} are the transfer mobilities of the isolator. Note that K_{11}, K_{22}, K_{12} and K_{21} are the corresponding axial stiffnesses of the isolator. K_1 and K_2 are the stiffnesses of additional elastic elements attached to rigid masses a and b, respectively, for experimental purposes. Further, f_2 and f_3 are interfacial forces at connecting locations. The governing equations are

$$[\mathrm{j}\omega m_a + K_1/\mathrm{j}\omega]\, v_2 = -f_2 + f_1, \qquad [\mathrm{j}\omega m_b + K_2/\mathrm{j}\omega]\, v_3 = -f_3, \tag{34a, b}$$

$$[\mathrm{j}\omega m_a + K_1/\mathrm{j}\omega]\, v_2 = -f_2, \qquad [\mathrm{j}\omega m_b + K_2/\mathrm{j}\omega]\, v_3 = -f_3 + f_4, \tag{34c, d}$$

$$v_2 = \beta_{22} f_2 + \beta_{23} f_3, \qquad v_3 = \beta_{32} f_2 + \beta_{33} f_3. \tag{34e, f}$$

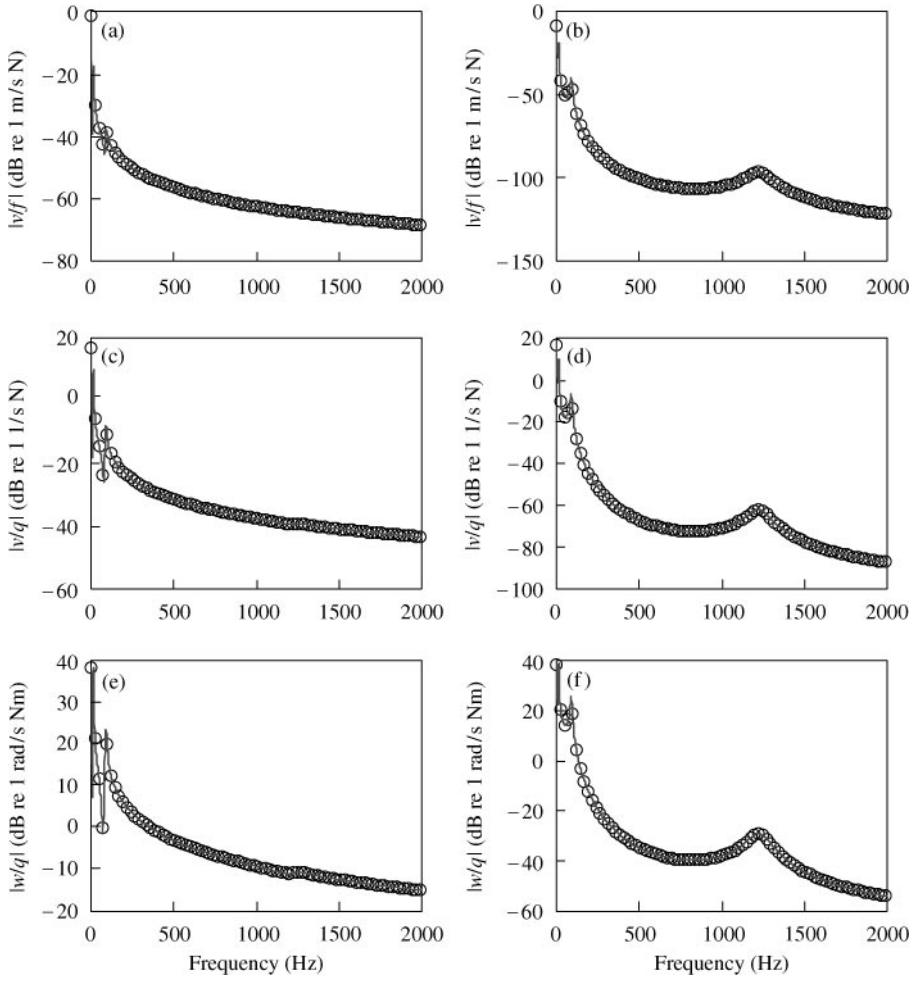

Figure 7. Synthesized mobilities for a system consisting of two rigid masses and an elastic beam as shown in Figure 2(b). (a) driving point force mobility; (b) driving point coupling mobility; (c) driving point moment mobility; (d) transfer force mobility; (e) transfer coupling mobility; (f) transfer moment mobility. Key: ———, synthesized mobility; ○, direct analytical solution.

Using equations (34a–f) and eliminating interfacial forces, the following equations are obtained when an external force (f_1) is applied at rigid mass a:

$$\beta_{22}[\mathrm{j}\omega m_a + K_1/\mathrm{j}\omega + 1/\beta_{22}]\, v_2 + \beta_{23}[\,\mathrm{j}\omega m_b + K_2/\mathrm{j}\omega]\, v_3 = \beta_{22} f_1, \tag{35a}$$

$$\beta_{32}[\,\mathrm{j}\omega m_a + K_1/\mathrm{j}\omega]\, v_2 + \beta_{33}[\mathrm{j}\omega m_b + K_2/\mathrm{j}\omega + 1/\beta_{33}]\, v_3 = \beta_{32} f_1. \tag{35b}$$

The simultaneous solution of equations (35a, b) yields the driving point and transfer mobilities:

$$M_{11} = v_1/f_1 = \frac{[\mathrm{j}\omega m_b + K_2/\mathrm{j}\omega]\,[\beta_{22}\beta_{33} - \beta_{23}\beta_{32}] + \beta_{22}}{\Delta(\omega)}, \tag{36a}$$

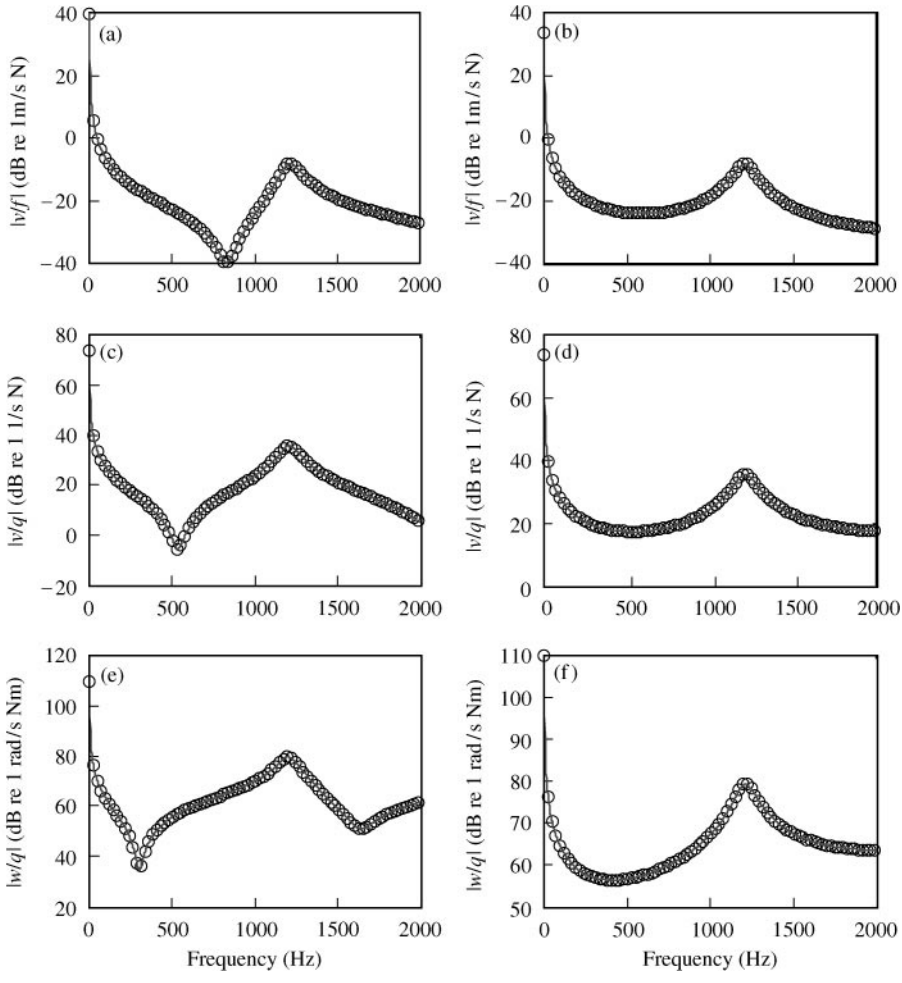

Figure 8. Decomposed mobilities for a beam using a system consisting of two rigid masses and an elastic beam as shown in Figure 2(b): (a) driving point force mobility; (b) driving point coupling mobility; (c) driving point moment mobility; (d) transfer force mobility; (e) transfer coupling mobility; (f) transfer moment mobility. Key: ———, decomposed mobility; ○, direct analytical solution.

$$M_{41} = v_4/f_1 = \frac{\beta_{32}}{\Delta(\omega)}, \tag{36b}$$

where

$$\Delta(\omega) = (\mathrm{j}\omega m_a + K_1/\mathrm{j}\omega)\beta_{22} + (\mathrm{j}\omega m_b + K_2/\mathrm{j}\omega)\beta_{22} + (\mathrm{j}\omega m_a + K_1/\mathrm{j}\omega)(\mathrm{j}\omega m_b + K_2/\mathrm{j}\omega)[\beta_{22}\beta_{33} - \beta_{23}\beta_{32}] + 1. \tag{36c}$$

In a similar manner, governing equations and mobilities are written as follows when an external force (f_4) is applied at rigid mass b:

$$\beta_{22}[\mathrm{j}\omega m_a + K_1/\mathrm{j}\omega + 1/\beta_{22}]v_2 + \beta_{23}[\mathrm{j}\omega m_b + K_2/\mathrm{j}\omega]v_3 = \beta_{23}f_4, \tag{37a}$$

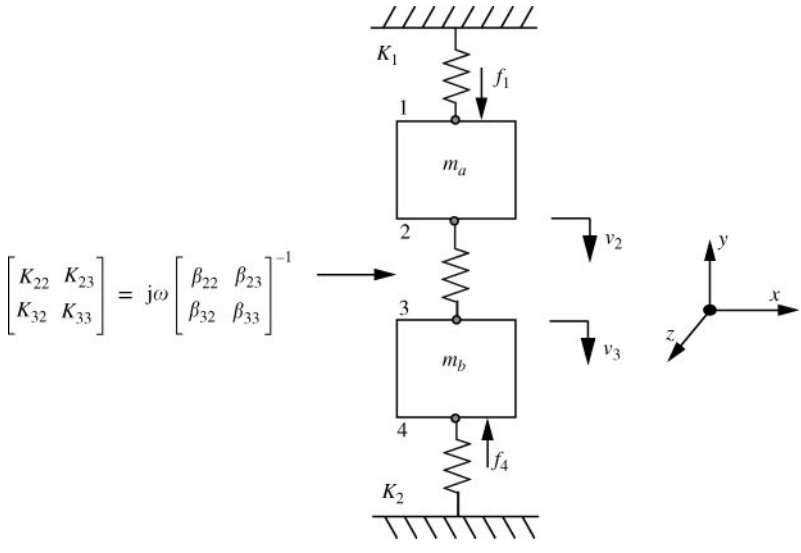

Figure 9. Discrete model of the physical system used to examine approximate methods.

$$\beta_{32}[\mathrm{j}\omega m_a + K_1/\mathrm{j}\omega]v_2 + \beta_{33}[\mathrm{j}\omega m_b + K_2/\mathrm{j}\omega + 1/\beta_{33}]v_3 = \beta_{33}f_4, \tag{37b}$$

$$M_{14} = v_1/f_4 = \frac{\beta_{23}}{\Delta(\omega)} \tag{38a}$$

$$M_{44} = v_4/f_4 = \frac{[\mathrm{j}\omega m_a + K_1/\mathrm{j}\omega][\beta_{22}\beta_{33} - \beta_{23}\beta_{32}] + \beta_{33}}{\Delta(\omega)}. \tag{38b}$$

From equations (36a, b), the motion transmissibility between two rigid masses is

$$\frac{v_4}{v_1} = \frac{\beta_{32}}{[\mathrm{j}\omega m_b + K_2/\mathrm{j}\omega][\beta_{22}\beta_{33} - \beta_{23}\beta_{32}] + \beta_{22}} = \frac{-K_{32}}{K_2 + K_{33} - m_b\omega^2}. \tag{39}$$

From the above transmissibility, transfer stiffness of an isolator K_{32} is extracted by assuming that $(K_2 + K_{33}) \ll \omega^2 m_b$ at high frequencies such that $\omega > \omega'$ where $\omega' = 3\sqrt{(K_2 + K_{33})/m_b}$, as reported by Thompson *et al.* [12]:

$$K_{32} \approx (-\omega^2 m_b)\frac{v_4}{v_1} \quad \text{for } \omega > \omega'. \tag{40}$$

This approximate method provides reasonable results for the transfer stiffness at higher frequencies, but yields a poor estimation at lower frequencies ($\omega > \omega'$). In order to enhance the identification scheme at low frequencies, the following transfer function is introduced in place of the typical motion transmissibility term [12]:

$$\frac{v_4}{v_1 - v_4} = \frac{\beta_{32}}{[\mathrm{j}\omega m_b + K_2/\mathrm{j}\omega][\beta_{22}\beta_{33} - \beta_{23}\beta_{32}] + \beta_{22} + \beta_{32}} = \frac{-K_{32}}{K_2 - m_b\omega^2 + K_{33} - K_{32}}. \tag{41}$$

From the above transfer function, the transfer stiffness is now approximated as follows by assuming that it is equal to the driving point stiffness, where $\omega'' = \sqrt{K_2/m_b}$ [12]:

$$K_{32} \approx (-\omega^2 m_b)\frac{v_4}{v_1 - v_4} \quad \text{for } \omega > \omega''. \tag{42}$$

6.3. APPROXIMATE METHOD FOR FLEXURAL MOTIONS

Unlike the analysis of Thompson *et al.* [12], now we examine this system in flexural motions. Again, we employ the mobility method where β_{22} and β_{33} are the driving point mobilities of the isolator; β_{23} and β_{32} are the transfer mobilities of the isolator in flexure. Further, K_{11}, K_{22}, K_{12} and K_{21} are corresponding flexural stiffnesses of the isolator. K_1 and K_2 are the flexural stiffnesses of additional elastic elements. Subscripts $x\theta$ and θx represent coupling mobilities or stiffnesses, and xx and $\theta\theta$ are used for diagonal terms. For rigid masses, h is the distance between the mass center and connecting locations of the isolator and I_G is the mass moment of inertia with respect to its mass center. Here f_2 and f_3 are interfacial forces and moments at connections, and f_{2e} and f_{3e} are external forces and q_{2e} and q_{3e} are external moments. The governing equations are

$$\mathrm{j}\omega m_a v_{1Gx} + [K_{1,xx}v_{1x} + K_{1,x\theta}w_1]/\mathrm{j}\omega = -f_{2x} + f_{2xe}, \tag{43a}$$

$$[\mathrm{j}\omega I_{aG}w_1 - \mathrm{j}\omega m_a h_a v_{1Gx}] + [-(K_{1,xx}v_{1x} + K_{1,x\theta}w_1)2h_a + K_{1,\theta x}v_{1x} + K_{1,\theta\theta}\mathrm{w}_1]/\mathrm{j}\omega = -q_2 + q_{2e}. \tag{43b}$$

$$\mathrm{j}\omega m_b v_{2Gx} + [K_{2,xx}v_{4x} + K_{2,x\theta}w_4]/\mathrm{j}\omega = -f_{3x}, \tag{43c}$$

$$[\mathrm{j}\omega I_{bG}w_1 - \mathrm{j}\omega m_b h_b v_{2Gx}] + [-(K_{2,xx}v_{4x} + K_{2,x\theta}w_4)2h_b + K_{2,\theta x}v_{4x} + K_{2,\theta\theta}w_4]\,\mathrm{j}\omega = -q_3, \tag{43d}$$

$$v_{2x} = \beta_{22,xx}f_{2x} + \beta_{22,x\theta}q_2 + \beta_{23,xx}f_{3x} + \beta_{23,x\theta}q_3, \tag{43e}$$

$$w_2 = \beta_{22,\theta x}f_{2x} + \beta_{22,\theta\theta}q_2 + \beta_{23,\theta x}f_{3x} + \beta_{23,\theta\theta}q_3, \tag{43f}$$

$$v_{3x} = \beta_{32,xx}f_{2x} + \beta_{32,x\theta}q_2 + \beta_{33,xx}f_{3x} + \beta_{33,x\theta}q_3, \tag{43g}$$

$$w_3 = \beta_{32,\theta x}f_{2x} + \beta_{32,\theta\theta}q_2 + \beta_{33,\theta x}f_{3x} + \beta_{33,\theta\theta}q_3. \tag{43h}$$

The equations of motion can be represented in matrix form

$$\left[\mathrm{j}\omega\mathbf{m}_a + \frac{1}{j\omega}\mathbf{K}_1\right]\mathbf{V}_2 = -\mathbf{F}_2 + \mathbf{F}_{2e}, \qquad \left[\mathrm{j}\omega\mathbf{m}_b + \frac{1}{j\omega}\mathbf{K}\right]\mathbf{V}_3 = -\mathbf{F}_3, \tag{44a, b}$$

$$\mathbf{V}_2 = \boldsymbol{\beta}_{22}\mathbf{F}_2 + \boldsymbol{\beta}_{23}\mathbf{F}_3, \qquad \mathbf{V}_3 = \boldsymbol{\beta}_{32}\mathbf{F}_2 + \boldsymbol{\beta}_{33}\mathbf{F}_3, \tag{44c, d}$$

where

$$\mathbf{m}_a = \begin{bmatrix} m_a & -m_a h_a \\ -m_a h_a & I_{aG} + m_a h_a^2 \end{bmatrix}, \qquad \mathbf{m}_b = \begin{bmatrix} m_b & m_b h_b \\ m_b h_b & I_{bG} + m_b h_b^2 \end{bmatrix}, \tag{44e, f}$$

$$\mathbf{K}_1 = \frac{1}{\mathrm{j}\omega}\begin{bmatrix} K_{1,xx} & -2h_a K_{1,xx} + K_{1,x\theta} \\ -2h_a K_{1,xx} + K_{1,\theta x} & 4h_a^2 K_{1,xx} - 2h_a(K_{1,x\theta} + K_{1,\theta x}) + K_{1,\theta\theta} \end{bmatrix}, \tag{44g}$$

$$\mathbf{K}_2 = \frac{1}{\mathrm{j}\omega}\begin{bmatrix} K_{2,xx} & 2h_b K_{2,xx} + K_{2,x\theta} \\ 2h_b K_{2,xx} + K_{2,\theta x} & 4h_b^2 K_{2,xx} + 2h_b(K_{2,x\theta} + K_{2,\theta x}) + K_{2,\theta\theta} \end{bmatrix}, \tag{44h}$$

$$\boldsymbol{\beta}_{22} = \begin{bmatrix} \beta_{22,xx} & \beta_{22,x\theta} \\ \beta_{22,\theta x} & \beta_{22,\theta\theta} \end{bmatrix}, \qquad \boldsymbol{\beta}_{23} = \begin{bmatrix} \beta_{23,xx} & \beta_{23,x\theta} \\ \beta_{23,\theta x} & \beta_{23,\theta\theta} \end{bmatrix}, \tag{44i, j}$$

$$\boldsymbol{\beta}_{32} = \begin{bmatrix} \beta_{32,xx} & \beta_{32,x\theta} \\ \beta_{32,\theta x} & \beta_{32,\theta\theta} \end{bmatrix}, \qquad \boldsymbol{\beta}_{33} = \begin{bmatrix} \beta_{33,xx} & \beta_{33,x\theta} \\ \beta_{33,\theta x} & \beta_{33,\theta\theta} \end{bmatrix}, \tag{44k, l}$$

$$\mathbf{F}_2 = [f_2 \quad q_2], \qquad \mathbf{F}_3 = [f_3 \quad q_3], \qquad \mathbf{F}_{2e} = [f_{2e} \quad q_{2e}]. \tag{44m–o}$$

Similar to the axial case, interfacial forces are eliminated from equations (44a–d), and equations of motion are rewritten as

$$\left[\mathrm{j}\omega\mathbf{m}_a + \frac{1}{\mathrm{j}\omega}\mathbf{K}_1 + \boldsymbol{\beta}_{22}^{-1}\right]\mathbf{V}_2 + \boldsymbol{\beta}_{22}^{-1}\boldsymbol{\beta}_{23}\left[\mathrm{j}\omega\mathbf{m}_b + \frac{1}{\mathrm{j}\omega}\mathbf{K}_2\right]\mathbf{V}_3 = \mathbf{F}_{2e}, \tag{45a}$$

$$\left[\mathrm{j}\omega\mathbf{m}_a + \frac{1}{\mathrm{j}\omega}\mathbf{K}_1\right]\mathbf{V}_2 + \boldsymbol{\beta}_{32}^{-1}\boldsymbol{\beta}_{33}\left[\mathrm{j}\omega\mathbf{m}_b + \frac{1}{\mathrm{j}\omega}\mathbf{K}_2 + \boldsymbol{\beta}_{33}^{-1}\right]\mathbf{V}_3 = \mathbf{F}_{2e}. \tag{45b}$$

Finally, the motion transmissibility in flexural motion is obtained as follows using equation (45):

$$\left[[\boldsymbol{\beta}_{33} - \boldsymbol{\beta}_{32}\boldsymbol{\beta}_{22}^{-1}\boldsymbol{\beta}_{23}]^{-1} + \left[\mathrm{j}\omega\mathbf{m}_b + \frac{1}{\mathrm{j}\omega}\mathbf{K}_2\right]\right]^{-1}[\boldsymbol{\beta}_{22}\boldsymbol{\beta}_{32}^{-1}\boldsymbol{\beta}_{33} - \boldsymbol{\beta}_{23}]^{-1}\mathbf{V}_2 = \mathbf{V}_3. \tag{46}$$

Next, the stiffness matrix can be partitioned and represented by sub-matrices of the mobility matrix by using

$$\mathbf{K} = \begin{bmatrix} \mathbf{K}_{22} & \mathbf{K}_{23} \\ \mathbf{K}_{32} & \mathbf{K}_{33} \end{bmatrix} = \mathrm{j}\omega\boldsymbol{\beta}^{-1} = \mathrm{j}\omega\begin{bmatrix} \boldsymbol{\beta}_{22} & \boldsymbol{\beta}_{23} \\ \boldsymbol{\beta}_{32} & \boldsymbol{\beta}_{33} \end{bmatrix}^{-1}$$

$$= \mathrm{j}\omega\begin{bmatrix} [\boldsymbol{\beta}_{22} - \boldsymbol{\beta}_{23}\boldsymbol{\beta}_{33}^{-1}\boldsymbol{\beta}_{32}]^{-1} & -[\boldsymbol{\beta}_{33}\boldsymbol{\beta}_{23}^{-1}\boldsymbol{\beta}_{22} - \boldsymbol{\beta}_{32}]^{-1} \\ -[\boldsymbol{\beta}_{22}\boldsymbol{\beta}_{32}^{-1}\boldsymbol{\beta}_{33} - \boldsymbol{\beta}_{23}]^{-1} & [\boldsymbol{\beta}_{33} - \boldsymbol{\beta}_{32}\boldsymbol{\beta}_{22}^{-1}\boldsymbol{\beta}_{23}]^{-1} \end{bmatrix}. \tag{47}$$

Using equation (47), the motion transmissibility can be represented in terms of stiffness matrices as

$$-[\mathbf{K}_2 - \omega^2\mathbf{m}_b + \mathbf{K}_{33}]^{-1}\mathbf{K}_{32}\mathbf{V}_2 = \mathbf{V}_3. \tag{48a}$$

Therefore, the transfer stiffness matrix of an isolator is approximated as follows where $(\mathbf{V}_3|\mathbf{V}_2)$ represents the velocity transmissibility between rigid masses a and b where | represents a complex quotient operation for matrices:

$$\mathbf{K}_{32} = \omega^2\mathbf{m}_b(\mathbf{V}_3|\mathbf{V}_2). \tag{48b}$$

Similarly, the transfer function matrix between $[\mathbf{V}_2 - \mathbf{V}_3]$ and $\mathbf{V}_3$ can be defined as

$$-[\mathbf{K}_2 - \omega^2\mathbf{m}_b + \mathbf{K}_{33} + \mathbf{K}_{32}]^{-1}\mathbf{K}_{32}(\mathbf{V}_2 - \mathbf{V}_3) = \mathbf{V}_3. \tag{49a}$$

Analogous to the identification of axial stiffness, the transfer stiffness matrix of the isolator in flexure is approximated from as follows, where $[\mathbf{V}_3|(\mathbf{V}_2 - \mathbf{V}_3)]$ represents the transfer function matrix that is by equation (49a):

$$\mathbf{K}_{32} = \omega^2\mathbf{m}_b[\mathbf{V}_3|(\mathbf{V}_2 - \mathbf{V}_3)]. \tag{49b}$$

6.4. SIMULATION EXAMPLE

In order to critically examine the generality of the original and refined schemes by Thompson *et al.* [12], a simulation example is chosen and symmetric and asymmetric isolators as shown in Figure 2(c) and (d) are examined. Axial (X) and flexural (Y) responses for the asymmetric isolator are written separately as follows where k_L and k_B are axial and flexural wave numbers of beams, respectively:

$$X_1(x, t) = X_1(x)e^{j\omega t} = \{A_{1L}\sin[k_{1L}x] + B_{1L}\cos[k_{1L}x]\}e^{j\omega t}, \tag{50a}$$

$$\begin{aligned} Y_1(x, t) &= Y_1(x)e^{j\omega t} \\ &= \{A_{1B}\sin[k_{1B}x] + B_{1B}\cos[k_{1B}x] + C_{1B}\sinh[k_{1B}x] + D_{1B}\cosh[k_{1B}x]\}e^{j\omega t}, \end{aligned} \tag{50b}$$

$$X_2(x, t) = X_2(x)e^{j\omega t} = \{A_{2L}\sin[k_{2L}x] + B_{2L}\cos[k_{2L}x]\}e^{j\omega t}, \tag{50c}$$

$$\begin{aligned} Y_2(x, t) &= Y_2(x)e^{j\omega t} \\ &= \{A_{2B}\sin[k_{2B}x] + B_{2B}\cos[k_{2B}x] + C_{2B}\sinh[k_{2B}x] + D_{2B}\cosh[k_{2B}x]\}e^{j\omega t}. \end{aligned} \tag{50d}$$

Here, subscripts 1 and 2 are used to represent the first and second beam, respectively, as shown in Figure 2(d). Harmonic responses of the asymmetric beam are then obtained by applying the following boundary conditions where $e^{j\omega t}$ is again dropped:

$$X_1(L_1) - X_2(L_1) = 0, \qquad S_1E_1\frac{dX_1(L_1)}{dx} + S_2E_2\frac{dX_2(L_1)}{dx} = 0, \tag{51a, b}$$

$$-S_1E_1\frac{dX_1(0)}{dx} = f_{x1}, \qquad S_2E_2\frac{dX_2(L_1 + L_2)}{dx} = f_{x2}, \tag{51c, d}$$

$$Y_1(L_1) - Y_2(L_1) = 0, \qquad \frac{dY_1(L_1)}{dx} - \frac{dY_2(L_1)}{dx} = 0, \tag{51e, f}$$

$$E_1I_{S1}\frac{d^2Y_1(L_1)}{d^2x} - E_2I_{S2}\frac{d^2Y_2(L_1)}{d^2x} = 0, \qquad E_1I_{S1}\frac{d^3Y_1(L_1)}{d^3x} - E_2I_{S2}\frac{d^3Y_2(L_1)}{d^3x} = 0, \tag{51g, h}$$

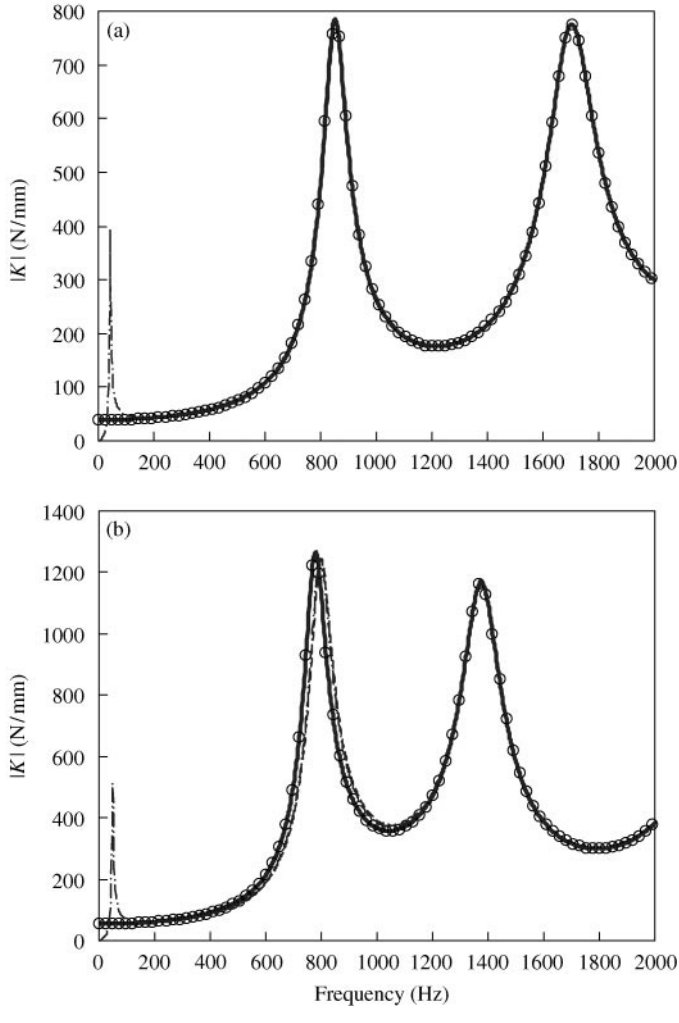

Figure 10. Decomposed axial stiffness for a beam using a system consisting of two rigid masses and an elastic beam as shown in Figure 2(b). (a) symmetric beam of Figure 2(c); (b) asymmetric beam of Figure 2(d). Key: ———, mobility synthesis method; — · — · —, approximate method using equation (40); - - - - -, approximate method using equation (42); ○, direct analytical solution.

$$E_1 I_{S1} \frac{\mathrm{d}^3 Y_1(0)}{\mathrm{d}x^3} = f_{y1}, \qquad -E_1 I_{S1} \frac{\mathrm{d}^2 Y_1(0)}{\mathrm{d}x^2} = q_1, \tag{51i,j}$$

$$-E_2 I_{S2} \frac{\mathrm{d}^3 Y_2(L_1 + L_2)}{\mathrm{d}x^3} = f_{y2}, \qquad E_2 I_{S2} \frac{\mathrm{d}^2 Y_2(L_1 + L_2)}{\mathrm{d}x^2} = q_2. \tag{51k,l}$$

Here f_{x1}, f_{x2}, f_{y1} and f_{y2} are external forces and q_1 and q_2 are external moments in equations (51c, d, i–l). For example, when the lateral force f_1 is applied at the free end of beam 1, $f_{y1} = f$ and $f_{x1} = f_{x2} = f_{y2} = q_1 = q_2 = 0$.

For the symmetric beam of Figure 2(c), the parameters of section 5.4 are used again for simulation. For the asymmetric beam case, the beam consists of two sections, as shown in Figure 2(d), of the same E, ρ and η as used previously. The radius and length of the first

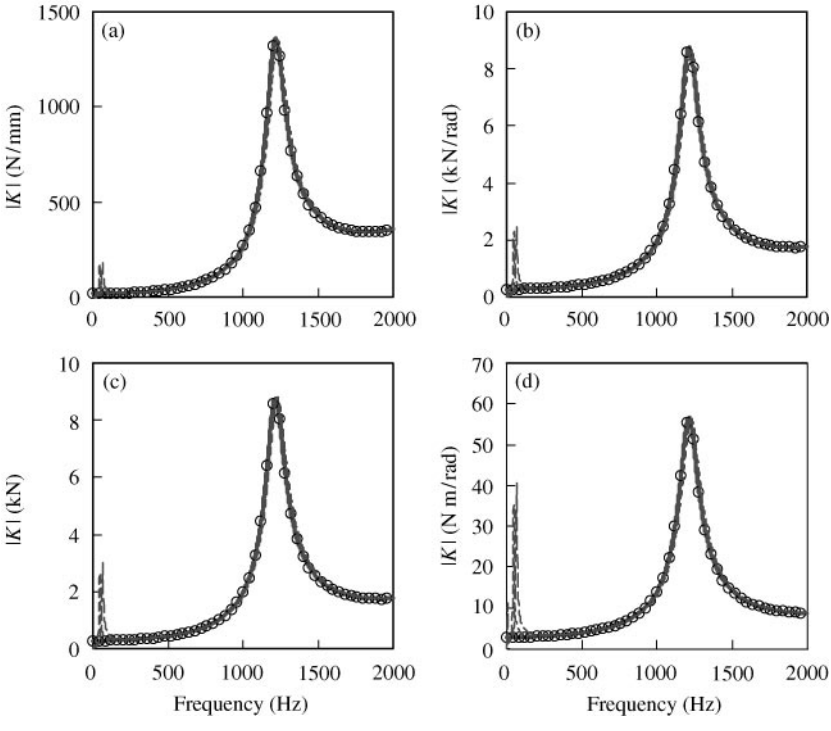

Figure 11. Decomposed flexural stiffnesses for the symmetric beam of Figure 2(c) using a system consisting of two rigid masses and an elastic beam as shown in Figure 2(b): (a) force stiffness; (b) coupling stiffness; (c) coupling stiffness; (d) moment stiffness. Key: ———, mobility synthesis method; — · — · —, approximate method using equation (48b); - - - - -, approximate method using equation (49b); ○, direct analytical solution.

section of the beam are 24 and 20 mm respectively. The dimensions of the second section of the beam are 12 and 20 mm for the radius and length respectively. Refer to section 5.4 for other information. Simulation results are shown in Figure 10 for axial stiffness and Figures 11 and 12 for flexural stiffnesses. In simulating these schemes, the system of Figure 2(b) is assumed to be free at both ends. Hence, the additional elastic elements, K_1 and K_2, are not used since this assumption should reduce inaccuracies that may exist in the identification results.

As seen in Figure 10(a), the refined identification scheme for axial stiffness based on equation (42) seems to exhibit good results at all frequencies for the symmetric isolator even though the transfer stiffness identified using equation (40) shows discrepancies in the low-frequency regime. However, as shown in Figure 10(b), deviations are observed in the asymmetric isolator results, based on both approximate identification schemes. Such deviations come from the approximations made in the identification schemes and the fact that the driving point and the transfer stiffnesses are not equal. In the identification of flexural stiffnesses, discrepancies at low frequencies are observed in either scheme based on equations (48b) or (49b) for both symmetric and asymmetric isolators as observed in Figures 11 and 12. The refined scheme does not suppress discrepancies at lower frequencies since the effect of the difference between the driving point and transfer stiffness matrices still remains imbedded. This is due to the coupling that is introduced by flexural motions. Also, it is seen that deviations are more pronounced for the asymmetric isolator at moderately high frequencies. Nonetheless, it should be noted that the discrepancies beyond the low-frequency regime could be reduced when a larger inertial element is used for mass *b*.

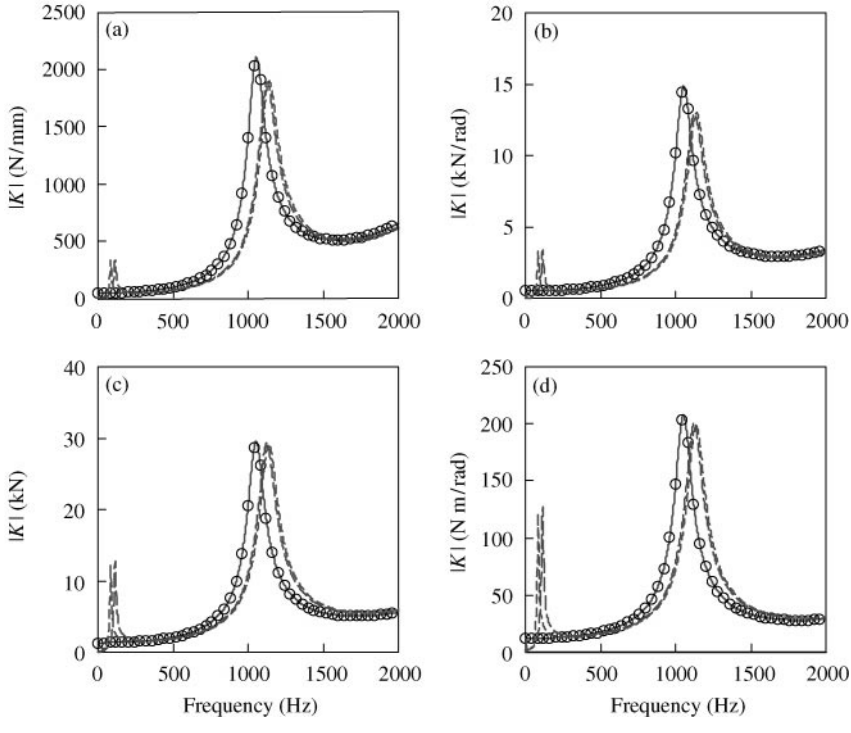

Figure 12. Decomposed flexural stiffnesses for the asymmetric beam of Figure 2(d) using a system consisting of two rigid masses and an elastic beam as shown in Figure 2(b): (a) force stiffness; (b) coupling stiffness; (c) coupling stiffness; (d) moment stiffness. Key: ———, mobility synthesis method; — · — · —, approximate method using equation (48b); – – – –, approximate method using equation (49b); ○, direct analytical solution.

7. IDENTIFICATION OF MOBILITY MATRIX OF AN ISOLATOR

7.1. METHODOLOGY

The multi-dimensional mobility matrix of a vibration isolator can be identified using the proposed mobility synthesis formulation. Multi-degree-of-freedom connections at both ends of an isolator are modelled since information at both ends of a sub-system would be needed. Therefore, the transfer mobility matrix has to be identified in addition to the driving point mobility matrix. Two masses are attached to an isolator as depicted in Figure 2(a) and the synthesized mobility for the overall system is formulated first. Then the mobility matrix of an isolator is reformulated given the synthesized formulation. Finally, the mobility matrix of an isolator can be obtained by substituting the synthesized mobility matrix with the measured mobility matrix for the combined system. It is possible to measure all elements of the multi-dimensional mobility matrix from the fact that an application of force with an offset from the reference point results in both force and moment simultaneously. Experiments have to be performed at all of the degrees of freedom that need to be identified. Also, each excitation has to include at least one different degree of freedom. For example, two excitations are needed to describe force and moment. Therefore, one excitation has to include a dynamic force and the other excitation must include a dynamic moment for a beam in flexure. This is obvious from the fact that responses and consequently the mobility cannot be obtained without appropriately exciting the degree of freedom in

question. Consequently, one must design a test matrix such that frequency responses yield the appropriate diagonal and non-diagonal terms.

In order to examine the proposed identification procedure in detail, recall Figure 1(b) that consists of three sub-systems. In this case, we need to identify mobilities $\boldsymbol{\beta}_{ij}$ of component (P). Therefore, mobilities $\mathbf{M}_{ij}$ of the combined system must be measured from specific experiments. The method assumes that $\boldsymbol{\alpha}_{ij}$ and $\boldsymbol{\gamma}_{ij}$ are well known, based on rigid body component theory. Here, $i, j = 2,3$ for $\boldsymbol{\beta}_{ij}$, 1,4 for $\mathbf{M}_{ij}$, 1,2 for $\boldsymbol{\alpha}_{ij}$ and 3,4 for $\boldsymbol{\gamma}_{ij}$. Also, relate $\boldsymbol{\beta}_{ij}$ and $\mathbf{M}_{ij}$ as

$$\begin{bmatrix}\mathbf{V}_1\\ \mathbf{V}_4\end{bmatrix} = \begin{bmatrix}\mathbf{M}_{11} & \mathbf{M}_{14}\\ \mathbf{M}_{41} & \mathbf{M}_{44}\end{bmatrix}\begin{bmatrix}\mathbf{F}_1\\ \mathbf{F}_4\end{bmatrix}, \qquad \begin{bmatrix}\mathbf{V}_2\\ \mathbf{V}_3\end{bmatrix} = \begin{bmatrix}\boldsymbol{\beta}_{22} & \boldsymbol{\beta}_{23}\\ \boldsymbol{\beta}_{32} & \boldsymbol{\beta}_{33}\end{bmatrix}\begin{bmatrix}\mathbf{F}_2\\ \mathbf{F}_3\end{bmatrix}. \tag{52a, b}$$

For a true three-dimensional motion, mobility matrices $\boldsymbol{\beta}_{ij}$ and $\mathbf{M}_{ij}$ are of dimension 6 and each matrix should be well populated since all motions are interrelated. However, we assume, for the sake of convenience, that each mobility matrix is composed of six diagonal terms and some coupling terms that link linear and angular motions in lateral directions. In other words, we assume that there does not exist any coupling between axial (x) and lateral motions (y and z) with reference to the co-ordinate system in Figure 1(a). Consequently, the mobility matrix $\boldsymbol{\beta}_{ij}$ of an isolator in three-dimensional motions has the components

$$\begin{bmatrix} v_x\\ v_y\\ v_z\\ w_x\\ w_y\\ w_z\end{bmatrix} = \begin{bmatrix} \tilde{M}_{xx}(\omega) & 0 & 0 & \tilde{M}_{x\theta_x}(\omega) & 0 & 0\\ 0 & \tilde{M}_{yy}(\omega) & \tilde{M}_{yz}(\omega) & 0 & \tilde{M}_{y\theta_y}(\omega) & \tilde{M}_{y\theta_z}(\omega)\\ 0 & \tilde{M}_{zy}(\omega) & \tilde{M}_{zz}(\omega) & 0 & \tilde{M}_{z\theta_y}(\omega) & \tilde{M}_{z\theta_z}(\omega)\\ \tilde{M}_{\theta_x x}(\omega) & 0 & 0 & \tilde{M}_{\theta_x\theta_x}(\omega) & 0 & 0\\ 0 & \tilde{M}_{\theta_y y}(\omega) & \tilde{M}_{\theta_y z}(\omega) & 0 & \tilde{M}_{\theta_y\theta_y}(\omega) & \tilde{M}_{\theta_y\theta_z}(\omega)\\ 0 & \tilde{M}_{\theta_z y}(\omega) & \tilde{M}_{\theta_z z}(\omega) & 0 & \tilde{M}_{\theta_z\theta_y}(\omega) & \tilde{M}_{\theta_z\theta_z}(\omega)\end{bmatrix}\begin{bmatrix} f_x\\ f_y\\ f_z\\ q_x\\ q_y\\ q_z\end{bmatrix}. \tag{53}$$

In this representation, the x-axis is the axial direction and the θ_x is the angular motion about the x-axis. Hence, the coupling terms in these directions vanish.

Next, consider the mobilities of the combined system. The concept of measuring rotation using translational velocities given moment excitation can be formulated in matrix form and the resulting mobilities for the combined system are

$$[\mathbf{M}_{11}] = [\mathbf{V}_{A1}][\mathbf{F}_{A1}]^{-1}, \qquad [\mathbf{M}_{14}] = [\mathbf{V}_{A1}][\mathbf{F}_{C4}]^{-1}, \tag{54a, b}$$

$$[\mathbf{M}_{41}] = [\mathbf{V}_{C4}][\mathbf{F}_{A1}]^{-1}, \qquad [\mathbf{M}_{44}] = [\mathbf{V}_{C4}][\mathbf{F}_{C4}]^{-1} \tag{54c, d}$$

where

$$[\mathbf{F}_{A1}] = [\mathbf{F}_{A1,1}\ \mathbf{F}_{A1,2}\ \mathbf{F}_{A1,3}\ \mathbf{F}_{A1,4}\ \mathbf{F}_{A1,5}\ \mathbf{F}_{A1,6}], \tag{54e}$$

$$[\mathbf{F}_{C4}] = [\mathbf{F}_{C4,1}\ \mathbf{F}_{C4,2}\ \mathbf{F}_{C4,3}\ \mathbf{F}_{C4,4}\ \mathbf{F}_{C4,5}\ \mathbf{F}_{C4,6}], \tag{54f}$$

$$[\mathbf{V}_{A1}] = [\mathbf{V}_{A1,1}\ \mathbf{V}_{A1,2}\ \mathbf{V}_{A1,3}\ \mathbf{V}_{A1,4}\ \mathbf{V}_{A1,5}\ \mathbf{V}_{A1,6}], \tag{54g}$$

$$[\mathbf{V}_{C4}] = [\mathbf{V}_{C4,1}\ \mathbf{V}_{C4,2}\ \mathbf{V}_{C4,3}\ \mathbf{V}_{C4,4}\ \mathbf{V}_{C4,5}\ \mathbf{V}_{C4,6}]. \tag{54h}$$

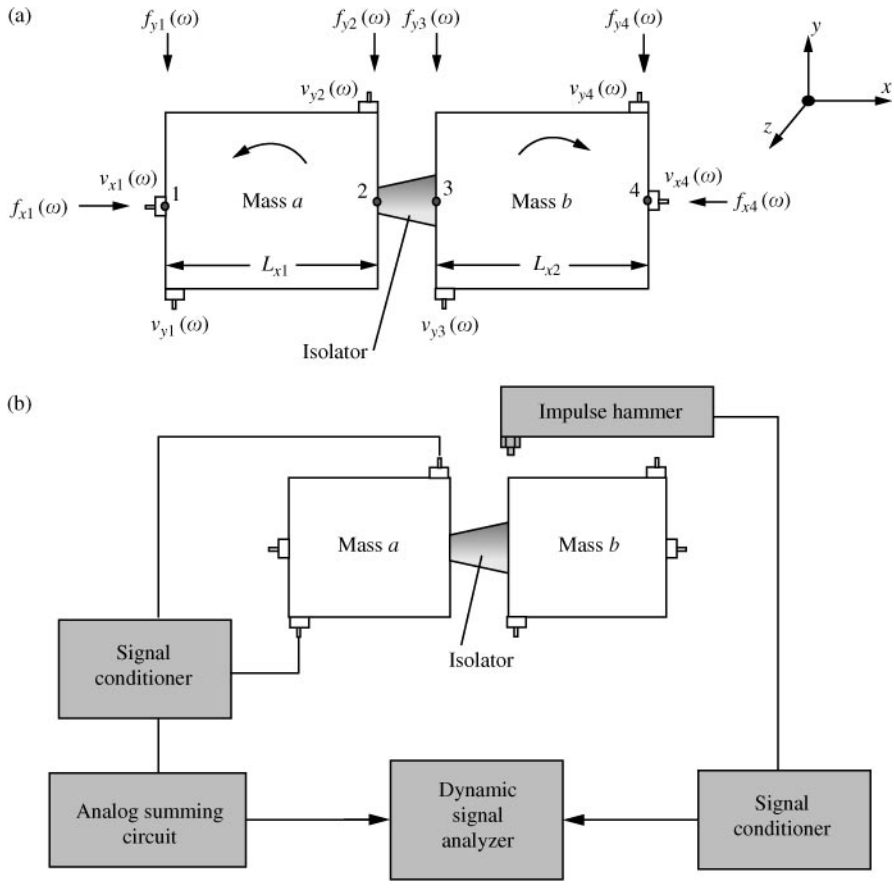

Figure 13. Experimental study used to identify mobilities of an isolator: (a) simplified model; (b) experimental schematic.

Here, subscripts $A1$ and $C4$ refer to excitations and responses at points 1 of system A and 4 of system C, and the third subscript from 1 to 6 (following the comma) indexes excitation and response vectors.

7.2. ILLUSTRATION OF THE PROCEDURE FOR PLANAR MOTIONS

As explained earlier, at least one excitation vector corresponding to the mobility matrix has to incorporate each degree of freedom. This is obvious from the fact that mobility for the corresponding degree of freedom cannot be obtained without an excitation for that degree of freedom. This requirement also corresponds to the existence condition for the inverse of excitation matrix (**F**). This procedure is based on the assumption that known sub-systems at either ends of an isolator are rigid bodies since this assumption allows us to relate translational responses to rotation responses. A simplified procedure for planar motion is shown in Figure 13(a).

First, one must select arbitrary reference locations within each rigid body. In Figure 13(a), locations 1 and 4 are designated as the reference points for masses 1 and 2, respectively, and locations 2 and 3 are designated as the interfaces between isolator with masses 1 and

TABLE 1

List of instruments used for experimental studies

Item	Manufacturer	Model No.
Accelerometer	PCB	A353B66
Impulse hammer	PCB	086B03
Analog summing circuit	In-house	—
Signal conditioner	PCB	480E09
Dynamic signal analyzer	HP	HP35670A
MTS testing system	MTS	831·50

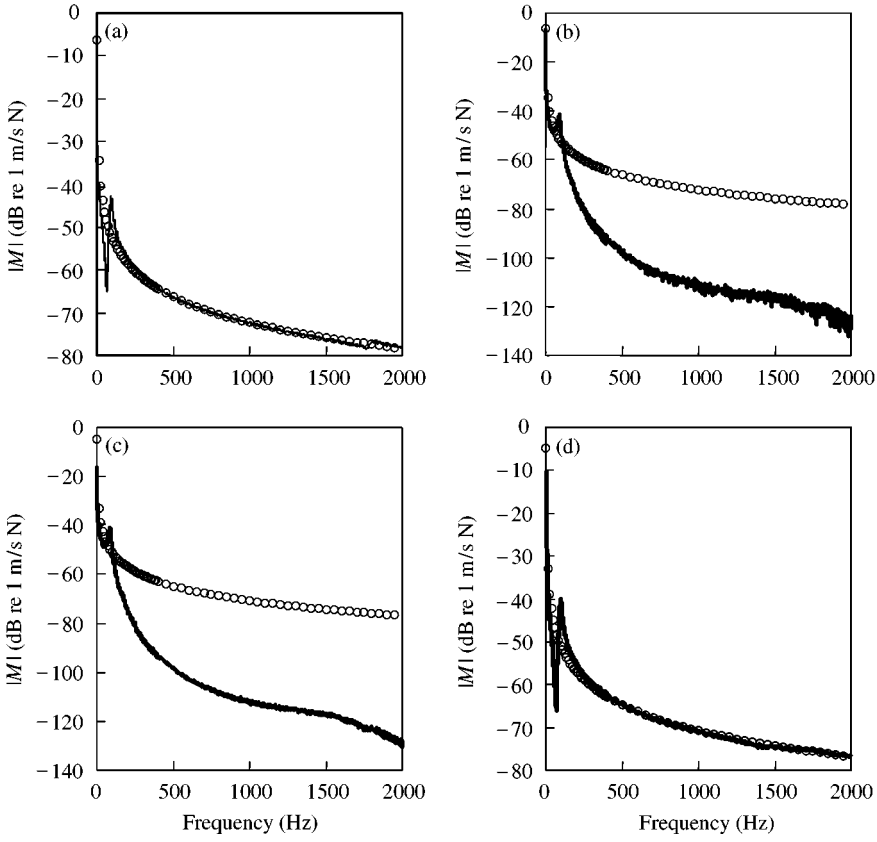

Figure 14. Measured mobility magnitudes for the system consisting of two rigid masses and isolator 1 in axial motion. (a) driving point mobility M_{11}; (b) transfer mobility M_{12}; (c) transfer mobility M_{21}; (d) driving point mobility M_{22}. Key: ———, measured; ○, predicted mass line.

2 respectively. The first task is to experimentally determine mobilities at reference points of the combined system, and then the mobilities of the isolator are decomposed from measured mobilities of the combined system using equations (8a–d). As explained earlier for three-dimensional motions, it is assumed that the axial motion (x-axis) of the isolator is uncoupled from its flexural motions (y and θ_z). Also, the small angle (θ) approximation ($\sin\theta \approx \tan\theta \approx \theta$ and $\cos\theta \approx 1$) for the rigid bodies is made. Mobilities at reference points

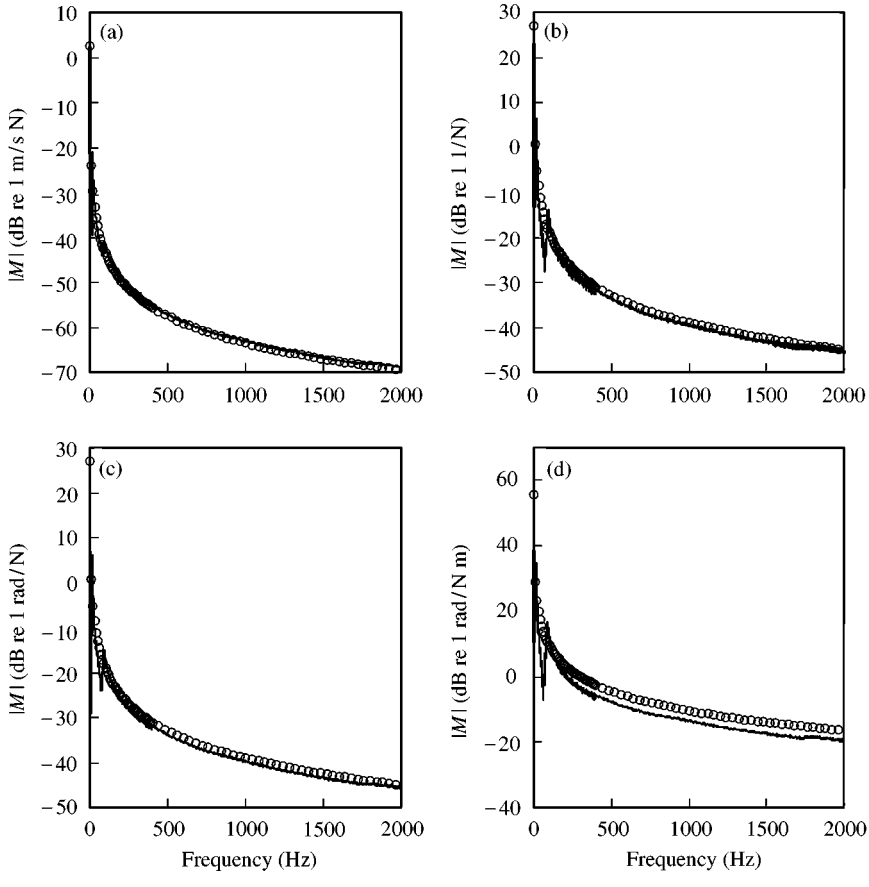

Figure 15. Measured driving point mobility magnitudes for the system consisting of two rigid masses and isolator 1 in flexural motion. (a) force mobility; (b) coupling mobility $M_{y\theta}$; (c) coupling mobility $M_{\theta y}$; (d) moment mobility. Key: ———, measured; ○, predicted mass line.

of the overall system in x direction are independent of the ones along the y- and θ_z-axis when the reference points are placed at the center of the rectangular masses along the y-axis. Therefore, excitation at reference locations 1 and 4 of the overall system along the x-axis does not generate any displacements along the y- and θ_z-axis. Here, it is further assumed that displacements of a rigid body in the y-axis are the same as those on a line parallel to the y-axis by the small angle approximation. For example, v_{y1} is used to describe the displacement of reference point 1 along the y-axis.

In order to determine mobilities of the combined system, three sets of measurements are needed for each mobility matrix in planar motions. First, for the measurement array of Figure 13(a), excitation and velocity sets for the mobility matrix $\mathbf{M}_{11}$ are as follows where subscripts after the comma refer to the excitation counts:

$$[\mathbf{F}_{A1,1}] = [f_{x1,1} \quad 0 \quad 0]^{\mathrm{T}}, \qquad [\mathbf{V}_{A1,1}] = [-v_{x1,1} \quad 0 \quad 0]^{\mathrm{T}}, \tag{55a, b}$$

$$[\mathbf{F}_{A1,2}] = [0 \quad -f_{y1,2} \quad 0]^{\mathrm{T}}, \qquad [\mathbf{V}_{A1,2}] = [0 \quad -v_{y1,2} \quad (v_{y1,2} + v_{y2,2})/L_{x1}]^{\mathrm{T}}, \tag{55c, d}$$

$$[\mathbf{F}_{A1,3}] = [0 \quad -f_{y2,3} \quad -L_{x1} f_{y2,3}]^{\mathrm{T}}, \qquad [\mathbf{V}_{A1,3}] = [0 \quad -v_{y1,3} \quad (v_{y1,3} + v_{y2,3})/L_{x1}]^{\mathrm{T}}. \tag{55e, f}$$

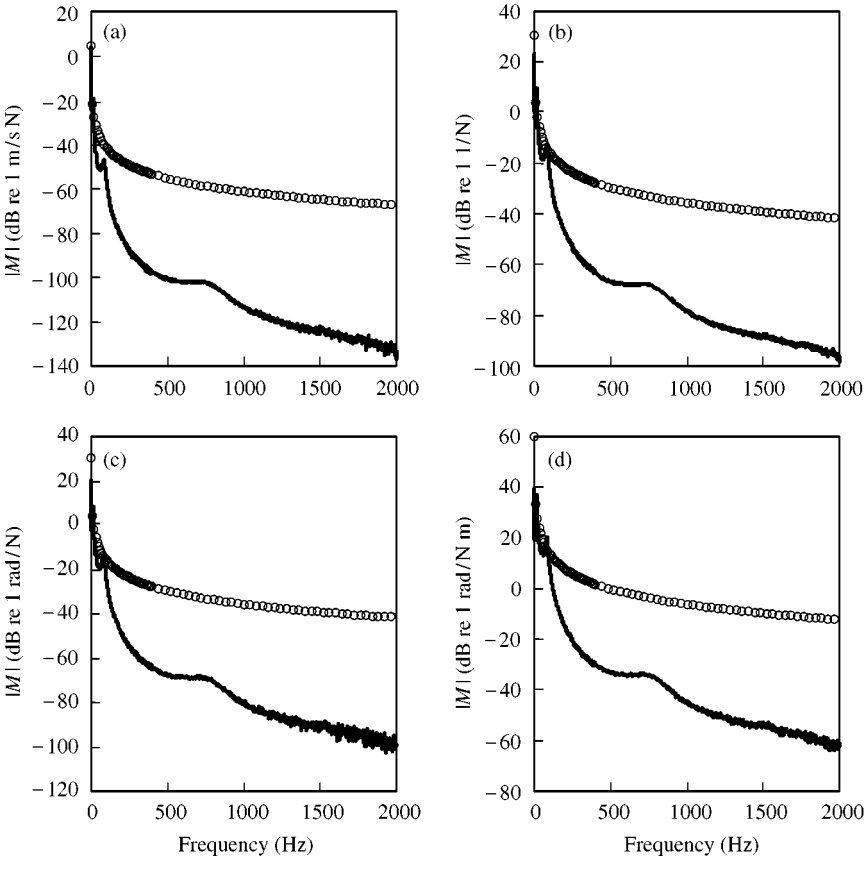

Figure 16. Measured transfer mobility magnitudes for the system consisting of two rigid masses and isolator 1 in flexural motion: (a) force mobility; (b) coupling mobility $M_{y\theta}$; (c) coupling mobility $M_{\theta y}$; (d) moment mobility. Key: ———, measured; ○, predicted mass line.

According to equations (54a) and (54e, f), the mobility matrix $\mathbf{M}_{11}$ is calculated using measured vectors as follows:

$$\mathbf{M}_{11} = \begin{bmatrix} \mathbf{M}_{11,xx} & \mathbf{M}_{11,xy} & \mathbf{M}_{11,x\theta} \\ \mathbf{M}_{11,yx} & \mathbf{M}_{11,yy} & \mathbf{M}_{11,y\theta} \\ \mathbf{M}_{11,\theta x} & \mathbf{M}_{11,\theta y} & \mathbf{M}_{11,\theta\theta} \end{bmatrix}$$

$$= \begin{bmatrix} -v_{x1,1} & 0 & 0 \\ 0 & -v_{y1,2} & -v_{y1,3} \\ 0 & (v_{y1,2}+v_{y2,2})/L_{x1} & (v_{y1,3}+v_{y2,3})/L_{x1} \end{bmatrix} \begin{bmatrix} f_{x1,1} & 0 & 0 \\ 0 & -f_{y1,2} & -f_{y2,3} \\ 0 & 0 & -L_{x1}f_{y2,3} \end{bmatrix}^{-1}. \quad (56)$$

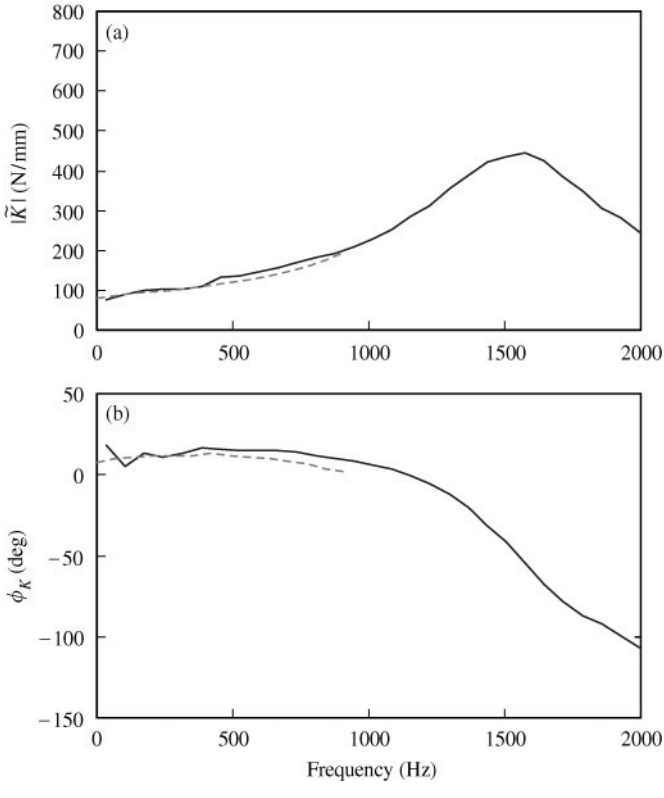

Figure 17. Comparison of axial dynamic stiffnesses for isolator 1. (a) dynamic stiffness modulus; (b) loss angle. Key: ———, mobility model; - - - - , measured (MTS): $f_{mean} = 1$ N.

For the sake of illustration, the mobility matrix $\mathbf{M}_{11}$ is rewritten as follows for harmonic excitations with unity amplitudes:

$$\mathbf{M}_{11} = \begin{bmatrix} v_{x1,1} & 0 & 0 \\ 0 & v_{y1,2} & v_{y1,3} \\ 0 & w_{z1,2} & w_{z1,3} \end{bmatrix} \begin{bmatrix} 1 & 0 & 0 \\ 0 & 1 & 1 \\ 0 & 0 & L_{x1} \end{bmatrix}^{-1}$$

$$= \begin{bmatrix} v_{x1,1} & 0 & 0 \\ 0 & v_{y1,2} & v_{y1,3} \\ 0 & w_{z1,2} & w_{z1,3} \end{bmatrix} \begin{bmatrix} 1 & 0 & 0 \\ 0 & 1 & -1/L_{x1} \\ 0 & 0 & 1/L_{x1} \end{bmatrix} = \begin{bmatrix} v_{x1,1} & 0 & 0 \\ 0 & v_{y1,2} & (v_{y1,3} - v_{y1,2})/L_{x1} \\ 0 & w_{z1,2} & (w_{y1,3} - w_{y1,2})/L_{x1} \end{bmatrix}. \tag{57}$$

Note that all measurements must be consistent in terms of sign convention though our analytical treatment assumes that all sensors provide data in the positive directions. Since the force excitation at reference point 2 can be replaced by a sum of force and moment at reference 1, responses at reference 1 are given by a linear superposition:

$$v_{y1,3} = \mathbf{M}_{11,yy} + \mathbf{M}_{11,y\theta} L_{x1}, \qquad w_{y1,3} = \mathbf{M}_{11,\theta y} + \mathbf{M}_{11,\theta\theta} L_{x1}. \tag{58a, b}$$

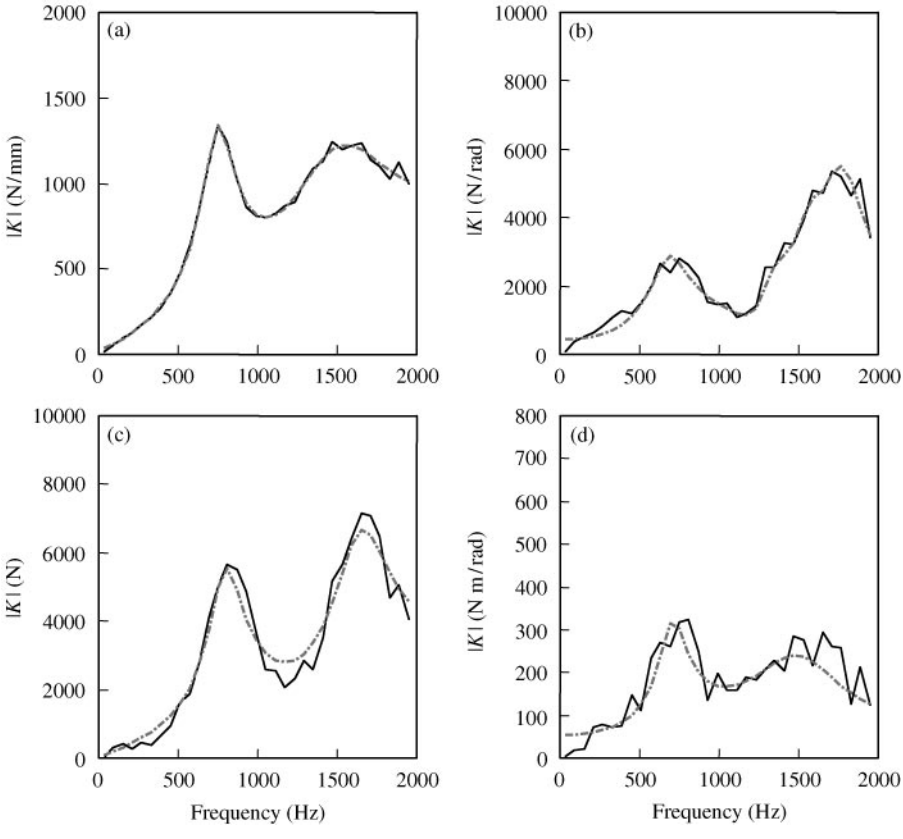

Figure 18. Transfer stiffnesses in flexural motion for isolator 1, as extracted using the identification scheme: (a) lateral stiffness modulus; (b) coupling stiffness modulus; (c) coupling stiffness modulus; (d) rotational stiffness. Key: ———, experimental result; — · — · —, curve fit.

Also, by noting that $v_{y1,2} = \mathbf{M}_{11,yy}$ and $w_{y1,2} = \mathbf{M}_{11,\theta y}$, and using the following relationships, it is seen that each element in the resulting equation (57) represents the corresponding component of $\mathbf{M}_{11}$:

$$(v_{y1,3} - v_{y1,2})/L_{x1} = (\mathbf{M}_{11,yy} + \mathbf{M}_{11,y\theta} L_{x1} - \mathbf{M}_{11,yy})/L_{x1} = \mathbf{M}_{11,y\theta}, \tag{59a}$$

$$(w_{y1,3} - w_{y1,2})/L_{x1} = (\mathbf{M}_{11,\theta y} + \mathbf{M}_{11,\theta\theta} L_{x1} - \mathbf{M}_{11,\theta y})/L_{x1} = \mathbf{M}_{11,\theta\theta}. \tag{59b}$$

Similarly, the following measurement sets are used to find the mobility matrix $\mathbf{M}_{14}$:

$$[\mathbf{F}_{A1,1}] = [f_{x1,1} \quad 0 \quad 0]^{\mathrm{T}}, \qquad [\mathbf{V}_{C4,1}] = [v_{x4,1} \quad 0 \quad 0]^{\mathrm{T}}, \tag{60a, b}$$

$$[\mathbf{F}_{A1,2}] = [0 \quad -f_{y1,2} \quad 0]^{\mathrm{T}}, \qquad [\mathbf{V}_{C4,2}] = [0 \quad v_{y4,2} \quad (v_{y3,2} + v_{y4,2})/L_{x2}]^{\mathrm{T}}, \tag{60c, d}$$

$$[\mathbf{F}_{A1,3}] = [0 \quad -f_{y2,3} \quad -L_{x1} f_{y2,3}]^{\mathrm{T}}, \qquad [\mathbf{V}_{C4,3}] = [0 \quad v_{y4,3} \quad (v_{y3,3} + v_{y4,3})/L_{x2}]^{\mathrm{T}}. \tag{60e, f}$$

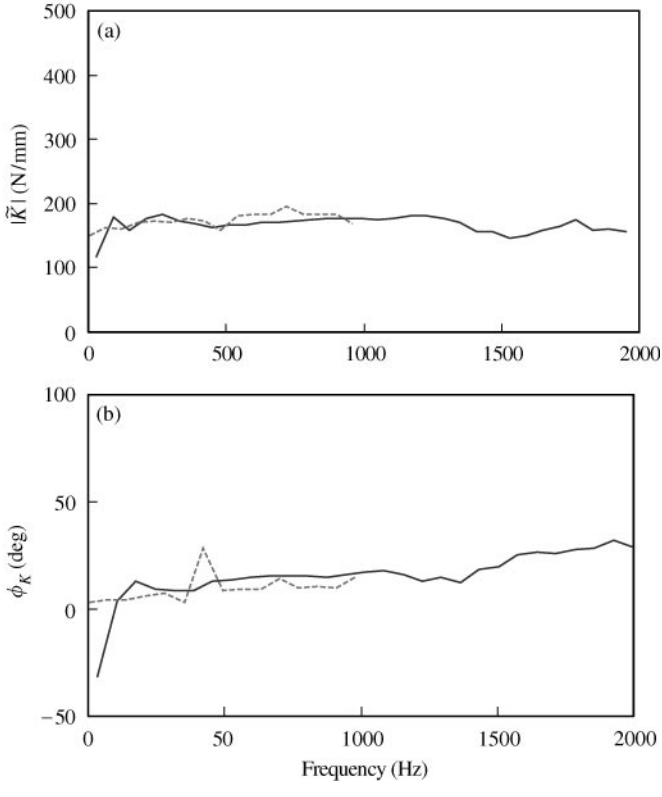

Figure 19. Comparison of axial dynamic stiffnesses for isolator 2. (a) dynamic stiffness modulus; (b) loss angle. Key: ———, mobility model; - - - - , measured (MTS): $f_{mean} = 2$ N.

A similar procedure is used for the mobility matrix $\mathbf{M}_{41}$:

$$[\mathbf{F}_{C4,4}] = [-f_{x4,4} \quad 0 \quad 0]^{\mathrm{T}}, \qquad [\mathbf{V}_{A1,1}] = [-v_{x1,4} \quad 0 \quad 0]^{\mathrm{T}}, \tag{61a, b}$$

$$[\mathbf{F}_{C4,5}] = [0 \quad -f_{y4,5} \quad 0]^{\mathrm{T}}, \qquad [\mathbf{V}_{A1,2}] = [0 \quad -v_{y1,5} \quad (v_{y1,5} + v_{y2,5})/L_{x1}]^{\mathrm{T}}, \tag{61c, d}$$

$$[\mathbf{F}_{C4,6}] = [0 \quad -f_{y3,6} \quad L_{x2} f_{y3,6}]^{\mathrm{T}}, \qquad [\mathbf{V}_{A1,3}] = [0 \quad -v_{y1,6} \quad (v_{y1,6} + v_{y2,6})/L_{x1}]^{\mathrm{T}}, \tag{61e, f}$$

For the mobility matrix $\mathbf{M}_{41}$, the following apply:

$$[\mathbf{F}_{C4,4}] = [-f_{x4,4} \quad 0 \quad 0]^{\mathrm{T}}, \qquad [\mathbf{V}_{C4,4}] = [v_{x4,4} \quad 0 \quad 0]^{\mathrm{T}}, \tag{62a, b}$$

$$[\mathbf{F}_{C4,5}] = [0 \quad -f_{y4,5} \quad 0]^{\mathrm{T}}, \qquad [\mathbf{V}_{C4,5}] = [0 \quad v_{y4,5} \quad (v_{y3,5} + v_{y4,5})/L_{x2}]^{\mathrm{T}}, \tag{62c, d}$$

$$[\mathbf{F}_{C4,6}] = [0 \quad -f_{y3,6} \quad L_{x2} f_{y3,6}]^{\mathrm{T}}, \qquad [\mathbf{V}_{C4,6}] = [0 \quad v_{y4,6} \quad (v_{y3,6} + v_{y4,6})/L_{x2}]^{\mathrm{T}}. \tag{62e, f}$$

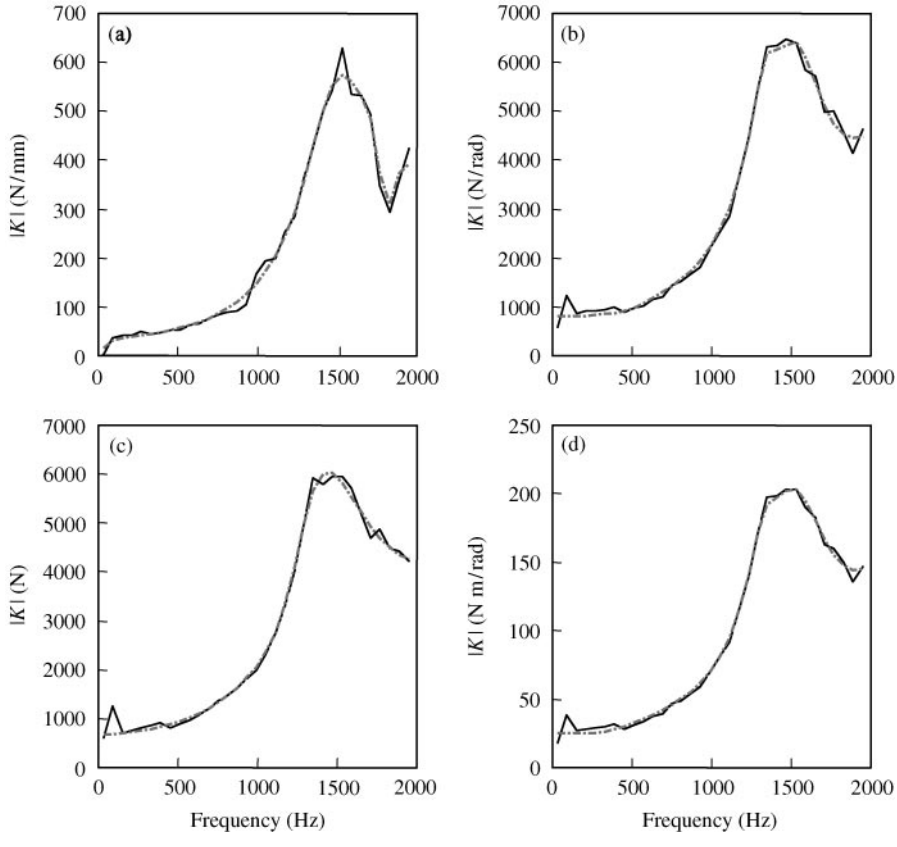

Figure 20. Transfer stiffnesses in flexural motion for isolator 2, as extracted using the identification scheme: (a) lateral stiffness modulus; (b) coupling stiffness modulus; (c) coupling stiffness modulus; (d) rotational stiffness. Key: ———, experimental result; — · — · —, curve fit.

Finally, mobility matrices of an isolator are calculated using equations (16, 17) and (24, 25) given the measured mobility matrices of the combined system and the analytical formulation for rigid bodies. Dynamic stiffness matrices of this isolator can then be obtained by using equation (47) when needed.

8. EXPERIMENTAL STUDIES

8.1. EXPERIMENTAL SYSTEM AND MEASUREMENT SAMPLES

Mobility models for three rubber isolators are identified using the proposed procedure. Two masses are attached to the ends of each isolator and the combined system of Figure 2(a) is suspended to simulate free boundaries. See section 5.4 for information on masses a and b used for experimental work. The reciprocity principle has been applied throughout the synthesis procedure since small inconsistencies or noise in frequency response function measurements can significantly contaminate results via the numerical inversion process that is essential to the entire procedure. Figure 13(b) shows a schematic that is used for experimental work; refer to Table 1 for a listing of instruments. The impulse hammer is used

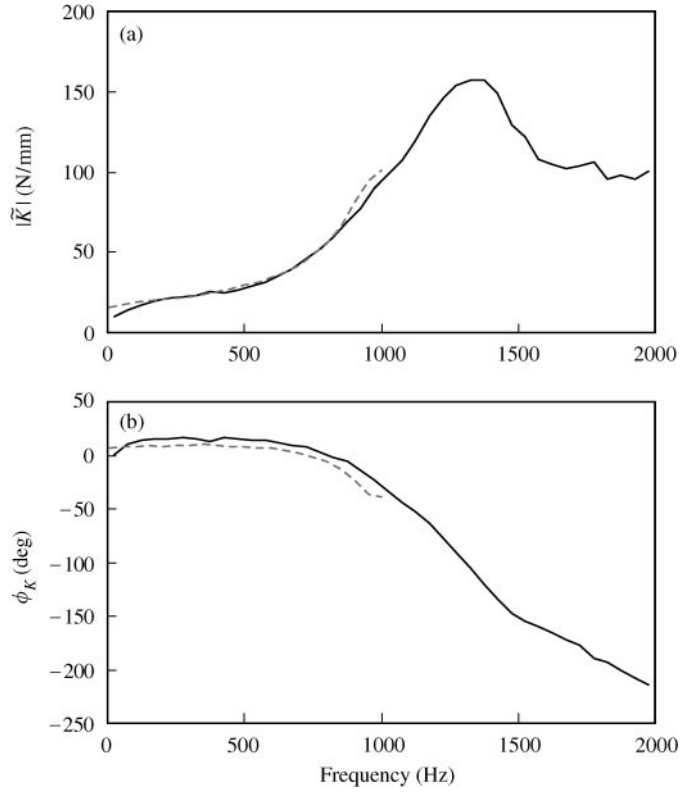

Figure 21. Comparison of axial dynamic stiffnesses for isolator 3: (a) dynamic stiffness modulus; (b) loss angle. Key: ———, mobility model; - - - - , measured (MTS): $f_{mean} = 3$ N.

for force excitation and five spectra (up to 2 kHz) are averaged for each measurement. An analog summing circuit is used to decompose the translational accelerations acquired at two opposite locations into rotational motions.

Measured mobilities of the combined system with isolator 1 are shown in Figure 14 for longitudinal motions, along with mobilities of rigid masses used for experimental work. Observe that the driving point mobilities converge to a mass line as frequency increases, unlike the transfer mobilities. Also, flexural mobilities of the combined system with isolator 1 are shown in Figure 15 for the driving point and in Figure 16 for the transfer point, along with mobilities of the rigid masses used.

8.2. RESULTS AND VALIDATION

Measurements of mobilities for the combined system are performed by acquiring acceleration data from rigid masses. From this measured set, moblity matrices at the reference points of the combined system are obtained using equations (54a–d). In our study, the reference points are set at the extreme ends of the combined system. Then, mobility matrices of the isolator in question are calculated using equations (16, 17) and (24, 25), and subsequently dynamic stiffness matrices are obtained from equation (58).

The typical results for transfer stiffnesses are shown in Figures 17–22 for three isolator examples of Figure 4. Note that the experimental validations, using the MTS 831.50

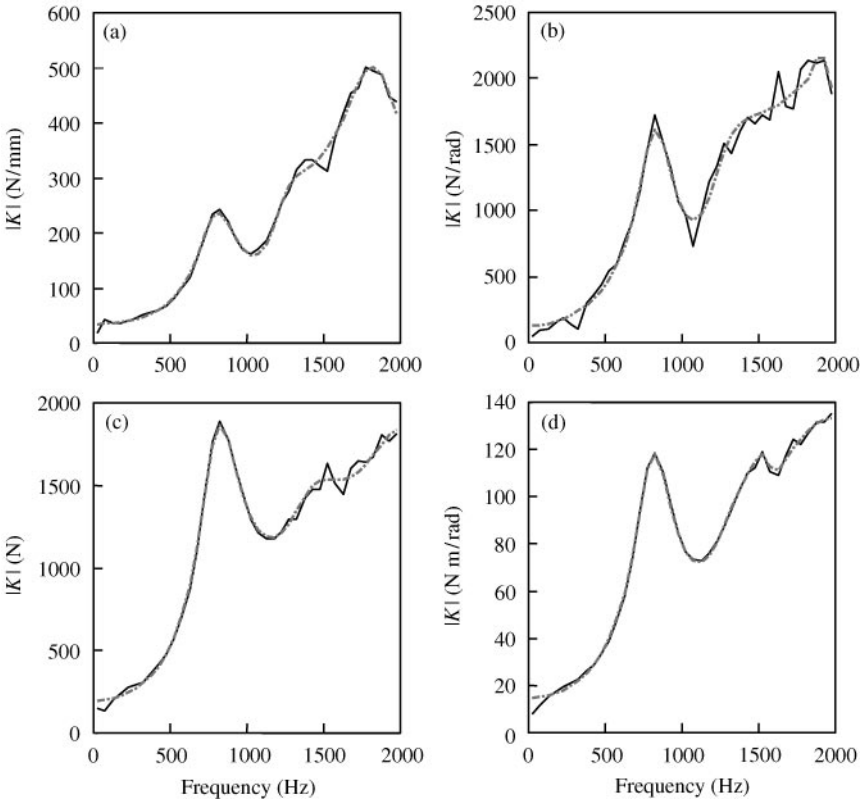

Figure 22. Transfer stiffnesses in flexural motion for isolator 3, as extracted using the identification scheme: (a) lateral stiffness modulus; (b) coupling stiffness modulus; (c) coupling stiffness modulus; (d) rotational stiffness. Key: ———, experimental result; — · — · —, curve fit.

machine, are conducted up to 1000 Hz. The MTS method [9] employs the blocked end boundary and only the transfer stiffness is measured. First, stiffness modulus and loss angle in axial direction are shown in Figures 17, 19 and 21. One may calculate loss factor (η) from loss angle (Φ) using the relationship $\eta = \tan \Phi$. Static stiffnesses in axial motions are 51, 130 and 5 N/mm for isolator 1, 2 and 3 respectively. Results identified from the proposed experiment are given up to 2000 Hz. Predictions for zero preload are compared with the MTS test results (with minimal preloads); these could only be obtained up to 1 kHz. Excellent agreements are observed between results based on the proposed identification method and experimental data yielded by the MTS machine. Further, predictions (with zero preload) are compared in Table 2 with measured results (at several small preloads). Observe that isolator 2 shows the preload-dependent stiffness, unlike isolators 1 and 3 that exhibit relatively insensitive stiffness to preloads. Next, stiffness moduli in flexural motions are shown in Figures 18, 20 and 22 for isolators 1, 2 and 3, respectively, along with their curve fits. The flexural stiffness modulus is curve fitted using a numerical function that employs the least-squares method in the frequency domain; one may establish a visco-elastic network model using such results. It is observed that the coupling stiffness moduli of symmetrical isolator 2 are almost identical, less than 10% difference, as shown in Figure 20 while the ones of Figures 18 and 22 are different for asymmetrical isolators 1 and 3. Note that the coupling terms of transfer stiffness are equal in magnitude for a symmetrical isolator but are different for an asymmetrical isolator. It is also observed in Figures 17–22

TABLE 2

Comparison of axial dynamic stiffnesses of isolators for various preloads

Isolator	Method	Preload (N)	Stiffness	100 Hz	300 Hz	500 Hz	700 Hz	930 Hz
1	Proposed	0	Stiffness modulus $\lvert\tilde{K}\rvert$ (N/mm)	90	103	137	160	201
	MTS	1		92	100	118	147	194
		5		105	118	138	166	202
		10		93	106	126	155	202
	Proposed	0	Loss angle Φ_K (deg)	5	13	14	14	8
	MTS	1		10	12	11	9	2
		5		11	13	13	11	6
		10		11	13	13	11	4
2	Proposed	0	Stiffness modulus	165	169	164	172	177
	MTS	2	$\lvert\tilde{K}\rvert$ (N/mm)	164	174	162	193	179
		63		204	210	214	218	213
		12		233	240	242	245	239
	Proposed	0	Loss angle Φ_K (deg)	4	9	13	15	15
	MTS	2		5	7	9	14	10
		63		4	7	9	10	10
		12		4	7	8	10	10
3	Proposed	0	Stiffness modulus $\lvert\tilde{K}\rvert$ (N/mm)	17	23	28	46	77
	MTS	3		18	22	30	42	86
		12		17	23	28	41	84
		23		16	20	27	40	83
	Proposed	0	Loss angle Φ_K (deg)	13	15	14	9	−14
	MTS	3		8	10	8	2	−26
		12		9	10	10	2	−27
		23		8	10	9	3	−28

that the wave effects occur within an isolator and therefore resonances are observed in stiffness spectra. For example, resonance at 1500 Hz in Figure 17(a) accounts for the wave effect of isolator 1.

9. CONCLUSION

A new characterization method has been proposed for the identification of multi-dimensional frequency-dependent transfer stiffnesses of an isolator. Our method uses a physical system that consists of two inertial elements and an isolator. Further, refined multi-dimensional mobility synthesis and decomposition procedures have been formulated. Our analytical framework removes some of the deficiencies of available synthesis models [18, 21, 22]. The results of the proposed scheme compare well with test data for three isolators in axial motions on a commercial machine up to 1 kHz. Also, approximate identification methods, as proposed by Thompson *et al.* [12], are critically analyzed for axial stiffnesses. The aforementioned method [12] is then extended to the identification of isolator stiffnesses in flexure. One simulation example is carried out for both symmetric and asymmetric isolators. Such approximate methods show some discrepancies from the exact stiffness up to certain transition frequency, depending upon the isolator, due to the

simplifications that are made in the formulation of such methods. For instance, this disagreement is pronounced for an asymmetric isolator.

The chief inherent limitation of our method is that the preload cannot be applied in the current configuration. This restriction must be overcome in a subsequent version of this method before applying it to assess practical devices. Refinements could incorporate a support structure, which may be either a very compliant base (made with a rubber-like material) or a massive block, in addition to the system of Figure 2(a). In case of a rubber base, the effect of elastic support on the mobility of the combined system of Figure 2(a) must be analytically examined to find possible approximations as the frequency increases. For a massive block-type support, the mobilities of the support must be experimentally obtained. The mobility of the combined system of Figure 2(a) should be decomposed such that support effects are excluded. The proposed analytical methodology could be conceptually refined to obtain the stiffness of an isolator. Future research should also consider the identification issues arising from the driving point stiffness at higher frequencies. Further, an investigation of correlation between laboratory and in situ measurements is desirable. Finally, non-linear effects need to be examined [17].

ACKNOWLEDGMENTS

The General Motors Corporation (Noise and Vibration Center) and the Goodyear Tire and Rubber Company (Transportation Molded Products) are gratefully acknowledged for supporting this research.

REFERENCES

1. C. M. HARRIS 1987 *Shock and Vibration Handbook*. New York: McGraw-Hill Book Company.
2. J. C. SNOWDON 1968 *Vibration and Shock in Damped Mechanical Systems*. New York: John Wiley & Sons, Inc.
3. A. D. NASHIF, D. I. G. JONES and J. P. HENDERSON 1986 *Vibration Damping*. New York: John Wiley & Sons, Inc.
4. J. I. SOLIMAN and M. G. HALLAM 1968 *Journal of Sound and Vibration* **8**, 329–351. Vibration isolation between non-rigid machines and non-rigid foundations.
5. H. G. D. GOYDER and R. G. WHITE 1980 *Journal of Sound and Vibration* **68**, 97–117. Vibrational Power flow from machines into built-up structures, Part III: power flow through isolation systems.
6. S. NADEAU and Y. CHAMPOUX 2000 *Experimental Techniques* May/June, 21–23. Application of the direct complex stiffness method to engine mounts.
7. L. F. NIELSEN, N. J. WISMER and S. GADE 2000 *Sound and Vibration* February, 20–24. An improved method for estimating the dynamic properties of materials.
8. T. JEONG 2000 *Ph.D. Thesis, The Ohio State University*. Analysis of powertrain mounts with focus on torque roll axis decoupling and frequency-dependent properties.
9. MTS Systems Corporation 1999 *Test Star II Control System User Manual—Dynamic Characterization*, p. 40.
10. D. J. THOMPSON and N. VINCENT 1995 *Vehicle System Dynamics Supplement* **24**, 86–99. Track dynamic behavior of at high frequencies. Part 1: theoretical models and laboratory measurements.
11. D. J. THOMPSON and J. W. VERHEIJ 1997 *Applied Acoustics* **52**, 1–17. The dynamic behavior of rail fasteners at high frequencies.
12. D. J. THOMPSON, W. J. VAN VLIET and J. W. VERHEIJ 1998 *Journal of Sound and Vibration* **213**, 169–188. Development of the indirect method for measuring the high frequency dynamic stiffness of resilient isolator.
13. A. FENANDER 1997 *Journal of Rail and Rapid Transit, Proceedings of I.Mech.E. Part F* **211**, 51–62. Frequency dependent stiffness and damping of railpads.

14. M. A. SANDERSON 1996 *Journal of Sound and Vibration* **198**, 171–191. Vibration isolation: moments and rotations included.
15. D. J. EWINS 1986 *Modal Testing: Theory and Practices*. Letchworth, U.K.: Research Studies Press.
16. L. CREMER, M. HECKLE and E. E. UNGAR 1973 *Structure-Bone Sound: Structural Vibrations and Sound Radiation at Audio Frequencies*: New York: Springer-Verlag.
17. C. M. RICHARDS and R. SINGH 2000 *Journal of Sound and Vibration*. Experimental characterization of rubber isolator nonlinearities in the context of single and multi-degree-of-freedom vibratory systems. (in press).
18. R. E. D. BISHOP and D. C. JOHNSON 1960 *The Mechanics of Vibration*. Cambridge: Cambridge University Press.
19. J. C. SNOWDON 1971 *Journal of Sound and Vibration* **15**, 307–323. Mechanical four-pole parameters and their application.
20. W. SOEDEL 1981 *Vibrations of Shells and Plates*. New York: Marcel Dekker, Inc.
21. T. E. ROOK and R. SINGH 1996 *Noise Control Engineering Journal* **44**, 69–78. Mobility analysis of structure-borne noise power flow through bearings in gearbox-like structures.
22. A. O. SYKES 1968 *Ph.D. Thesis, The Catholic University of America, Washington DC. U.S.A.* Development and application of linear multi-terminal network theory to vibration problems.

APPENDIX A: NOMENCLATURE

A, B, C, D	arbitrary constants
d	diameter
E	Young's modulus
f	force amplitude
$\mathbf{f}$	force amplitude vector
$\mathbf{F}$	excitation vector
G	shear modulus
h	reference location in rigid body with respect to mass center
$\mathbf{I}$	identity matrix
I_S	area moment of inertia
I_m	mass moment of inertia
j	$\sqrt{-1}$
k	wave number
K	stiffness
$\mathbf{K}$	stiffness matrix
L	length
m	mass
$\mathbf{m}$	inertia matrix
M	mobility
$\mathbf{M}$	mobility matrix
q	moment amplitude
$\mathbf{q}$	moment amplitude vector
$\mathbf{R}$	rotation matrix for the cross vector product
S	section area
S, P, R	source, path and receiver
$\mathbf{T}$	transformation matrix
X	displacement in x direction
Y	displacement in y direction
v	translational velocity
$\mathbf{v}$	translational velocity vector
$\mathbf{V}$	velocity vector
w	rotational velocity
$\mathbf{w}$	rotational velocity vector
x, y, z	cartesian co-ordinates
α, β, γ	mobilities of components
$\boldsymbol{\alpha}$, $\boldsymbol{\beta}$, $\boldsymbol{\gamma}$	mobility matrices of components
η	loss factor
θ	rotational displacement

ρ	density
Φ	loss angle, deg
ω	frequency, rad/s

Subscripts

G	mass center
a, b	mass a and b
B	flexural motion
i, j	indices or reference points in mass
L	axial or longitudinal motion
mean	mean load
S, P, R	source, path and receiver
v	translational component of mobility matrix of rigid body
w	rotational component of mobility matrix of rigid body
x, y, z	cartesian co-ordinates
1, 2, 3, 4	reference locations

Superscripts

T	transpose
$\sim$	complex valued
$'$,$''$	frequency used for criterion

Operators

Δ	determinant of system matrix
diag	diagonal matrix
|	complex quotient operation for matrices